UCLouvain

epl

École polytechnique de Louvain

Operation and control of isolated AC micro-grids for rural electrification in developing countries

Author: **Eduardo Rene Vasquez Mayen**
Supervisor: **Emmanuel De Jaeger**
Readers: **Guy Walongo Ndiwulu, Noël Janssens**
Academic year 2019–2020
Master [120] in Electrical Engineering

Abstract

While many advances have been done in terms of energy distribution, there is still a percentage of the population lacking access to electricity. In order to provide access to the missing sectors in the most economic way, the use of micro-grids has been proposed. The capability of micro-grids to operate disconnected from the main grid make them attractive for rural areas which are the most affected sectors. Due to the fact that these micro-grids are islanded, they have to set their own bus voltage and frequency. Different control schemes have been proposed in order to coordinate the voltage and frequency of the distributed generators (DG) which form the micro-grid. This thesis discusses two problems. First, the control methods for the distributed generators in a Low voltage (LV) grid are explored. Second, the mitigation of voltage unbalance caused by single phase loads is discussed.

This thesis focuses on two control schemes that do not require communication between converters. These are the "traditional" P.F/Q.V droop control and the "opposite" P.V/Q.F droop control. First, the improvement of using a virtual impedance is shown in each control scheme. Afterwards, through different tests their performance is assessed. The obtained results shown that the opposite droop control has a better performance than the traditional droop in mainly resistive lines such as the ones used in LV micro-grids.

Single phase loads can create a voltage unbalance. Due to the nature of the micro-grid, it can be difficult to reduce this unbalance. If left unattended the voltage unbalance will greatly decrease the power quality across the micro-grid. This thesis tests the effectiveness of a negative sequence compensation mechanism. This negative sequence compensation scheme is aimed at compensating voltage unbalance at the point of common coupling (PCC), but requires a low level of communication among DGs. This thesis explores the possibility of using this negative sequence compensation mechanism without any type of communication, and the effectiveness of such methods at a non-PCC location.

Acknowledgements

This work would not have been possible without the guidance provided by this thesis advisor professor Emmanuel De Jaeger. His doors have always remained open, and has always provided support to the best of his capabilities. Through his knowledge and insight into the problematic, he always helped improve the quality of the work while moving it into the correct direction.

I would also like to extend my gratitude to Guy Wanlongo Ndiwulu who provided several practical suggestions that helped overcome several difficulties in the project. I must also thank the international Lhoist Berghmans Innovation Chair as my studies at Université catholique de Louvain would not have been possible without their support.

Finally, I am truly grateful towards my family that have provided me with support and encouragement throughout this process. They have always motivated me to seek greater challenges, and to keep in pursue of knowledge and academic preparation. Without them none of this would be possible.

Contents

Acronyms

DG Distributed Generator.

ESMAP Energy Sector Management Assistance Program.

ESS Energy Storage System.

IEA International Energy Agency.

IEC International Electrotechnical Commission.

IEEE Institute of Electrical and Electronics Engineers.

IGBT Isolated Gate Bipolar Transistor.

ISO International Organization for Standardization.

LV Low Voltage.

MGCC Micro-grid Central Controller.

NS Negative Sequence.

P.F/Q.V Active Power.Frequency/Reactive Power.Voltage.

P.V/Q.F Active Power.Voltage/Reactive Power.Frequency.

PCC Point of Common Coupling.

PI Controller Proportional Integral Controller.

PS Positive Sequence.

PV Photo-voltaic.

PWM Pulse Width Modulation.

RMS Root Mean Square.

SGD7 Sustainable Development Goal 7.

UCR Unbalance Compensation Reference.

VSI Voltage Source Inverters.

VUF Voltage Unbalance Factor.

Nomenclature

δ	Power Angle
ε	Damping Ratio
*	Reference Value Superscript
$^+$	Positive Sequence Superscript
$^-$	Negative Sequence Superscript
$_{\alpha\beta}$	$\alpha\beta$ Reference Frame Subscript
$_{dq0}$	dq0 Reference Frame Subscript
C_ω	Control Block for Angular Frequency
C_E	Control Block for Voltage Amplitude
C_f	Filter Capacitance
C_P	Control Block for Active Power
C_Q	Control Block for Reactive Power
C_v	Control Block for Voltage
f	Frequency
f_g	Grid Frequency
f_{res}	Resonance Frequency
f_{sw}	Switching Frequency
i_g	Current Through Grid Side Inductance

K_p	Active Power Droop Coefficient
K_q	Reactive Power Droop Coefficient
l_g	Grid Side inductance
l_i	Inverter Side inductance
P	Active Power
Q	Reactive Power
R_d	Damping Resistance
V	Voltage
w	Angular Frequency
w_c	Angular Cut-off Frequency
wt	Rotating Frame
X	Reactance

Introduction

Although electricity has become an intrinsic part of our lives, there are still populations without access to it. Most of these sectors are located in developing countries in Asia and sub-Saharan Africa. Usually electricity is given to such sectors by extending the main grid. However, some regions may be isolated from the main grid due to distance or geographical features.

The constant increase in interest and efficiency on renewable energies have made a specific solution more viable for rural electrification. This solution is the concept of micro-grids. Micro-grids can be defined as local electrical networks that contain power generation units and power consumption units. The micro-grid has the responsibility to balance the supply and demand within it [1]. Micro-grids can operate connected to the main grid or by themselves in what is referred to as isolated/islanded mode. While operating in islanded mode, the micro-grid has to be able to sustain itself without any external connections. The power generation units consists of what are called Distributed generators (DG). These distributed generators are often renewable energies such as solar panels or wind turbines. Because of the inclusion of renewable energies, micro-grids also tackle the problematic regarding the increasing energy demand and the need to reduce the environmental foot print of energy generation. Micro-grid usage has been increasing as they provide an alternative that can lead to a sustainable development.

Most of the Distributed generators have an output at a voltage and frequency that is not the one traditionally used at the grid. Moreover, the outputted values differ depending on the source. Therefore each Distributed generator has to be interfaced by power electronics that bring the values to the standard values used on the grid. Because of the lack of inertial generators, the micro-grid has to be managed carefully so that it can handle changes to its structure without deviating from its ideal 50 Hz frequency. Additionally, in order to ensure quality of service to its users the micro-grid has to be able to sustain load changes, allow load sharing between distributed generators, and be able to sustain stability when providing single phase loads.

In this thesis micro-grids are studied under the context of rural electrification. The objective is to identify a suitable local control method for the distributed generators operating in a low voltage (LV) islanded micro-grid. Two main control types are analyzed. These are the P.F/Q.V droop control and the P.V/Q.F droop control. Finally, the stability of the grid under unbalance due to single phase loads is discussed. A negative sequence compensation mechanism is proposed, and its effectiveness is evaluated.

The master thesis has the following structure.

- Chapter 1 provides an overview to the state of rural electrification and the advances in renewable energies
- Chapter 2 describes the micro-grids and the main characteristics of an islanded micro-grid.
- Chapter 3 discusses the different distributed generator local control methods
- Chapter 4 describes the model used for simulation and discusses the results from applying the two different control methods on the micro-grid
- Chapter 5 discusses the effects of unbalanced loads on the micro-grid and how to possibly counter them using a negative sequence compensation mechanism

Chapter 1

State of rural electrification

Nowadays we associate the need of electricity with modern commodities such as smartphones, streaming services, and many other useful but not vital technologies. However, there is a still a substantial amount of communities that do not have access to electricity, and this deprives them from many basic quality of life improvements. Many efforts have been made to reduce the amount of people without access to electricity. However, by 2017 about 840 million people still did not have access to it [2]. As it can bee seen in figure 1.1 two major areas are suffering from lack of access to electricity. These areas are the Sub-Saharan Africa and South Asia. Providing electricity to these areas is key not only to provide them with quality of life improvements, but to help them develop as electricity has a key role in the development of such areas.

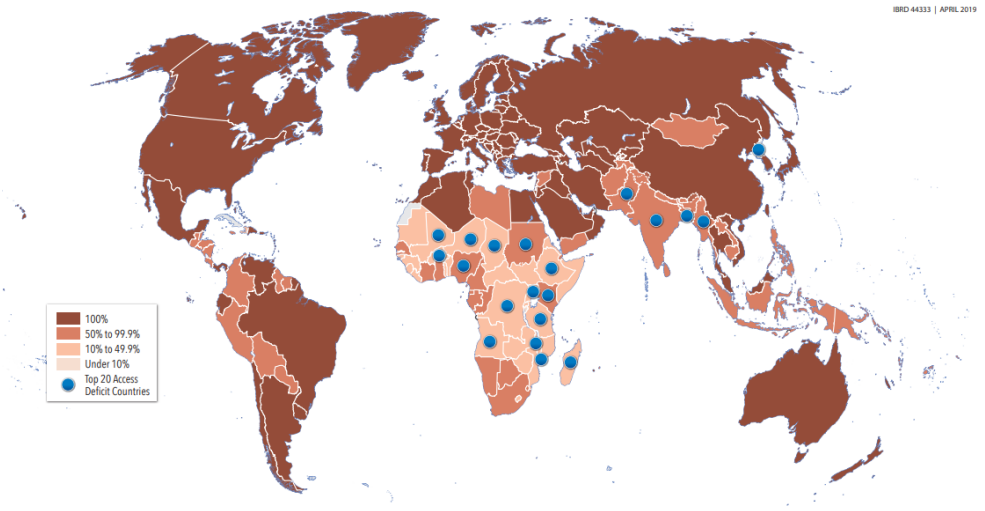

Figure 1.1: Share of population without access to electricity [2]

1.1 Rural areas

In order to evaluate the possible solutions, it is important to have a definition of what is a rural area. Rural areas are said to have common characteristics such as [3]:

- being a decentralized population
- being geographically isolated
- being under-served in terms of health care, education, clean water, sanitation, and other infrastructure
- being unable to participate in regional and national markets

Electrification takes a key role in such communities as it is strongly related to its development. When a community does not have access to electricity, a considerable part of their income has to be assigned to low quality and expensive energy sources such as kerosene and dry cell batteries [4]. The introduction of electricity can allow them to redirect their economical resources towards other areas. Additionally, the inclusion of a relatively simple element such as lighting increases safety, and provides good environments for studying and working. On a bigger scale it can lead to the inclusion of facilities such as medical clinics and schools [3].

When trying to provide rural areas with electricity the most common approach is to extend the existing main grid, but for some areas this option is not viable. As discussed before these areas are sometimes characterized by the fact that they are geographically isolated. Therefore the main grid is not able to reach to them. Under these circumstances micro-grids can be a long term sustainable solution to such problems.

1.2 Renewable energies

The increasing amount of carbon dioxide emissions has brought renewable energies into a new light as they can be a solution to reduce carbon emissions. At the same time, the increase in efficiency that some renewable energies have experienced has increased the interest and image of these energies. Not only have they obtained a better performance, but also their cost has decreased. Figure 1.2 compares the levelized cost of energy between 2010 and 2018. It can be seen that both solar and wind have seen significant reductions.

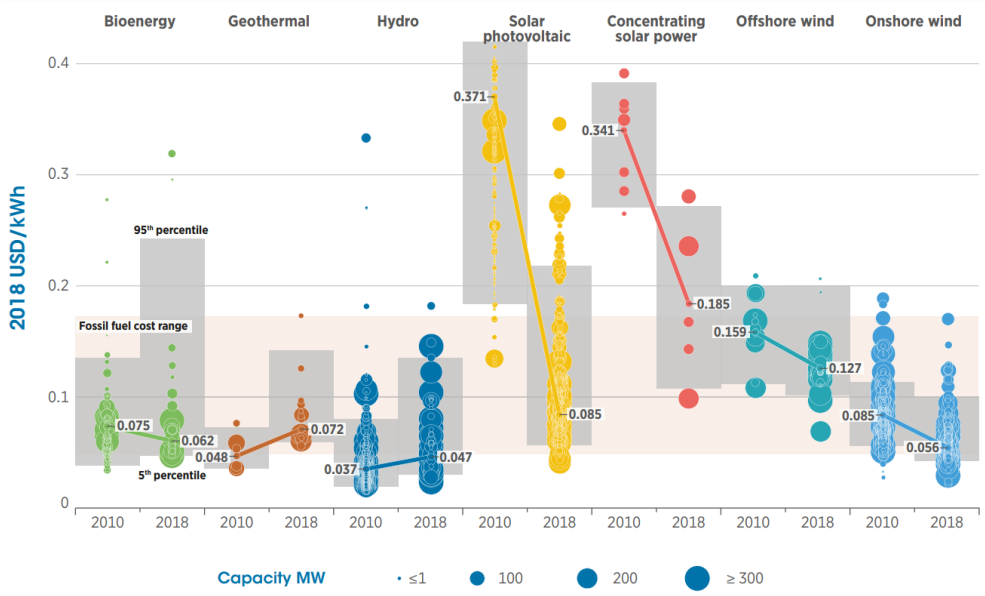

Figure 1.2: Global LCOE of utility-scale renewable power generation technologies, 2010–2018 [5]

Renewable energies can be used in three main end areas: electricity, heat, and transportation. Out of these three the electricity sector is the one experiencing the biggest growth which can be associated with the rapid development of wind and solar technologies [2]. According to the International Energy Agency (IEA) renewable energies will keep growing in the upcoming years. Figure 1.3 shows the amount of renewable energy capacity that has been added throughout recent years. It also predicts the amount that will be added in years to come. This shows that it is indeed expected that renewable energies will keep increasing. The mentioned accelerated case is what could happen if policies to push for renewable energies are implemented.

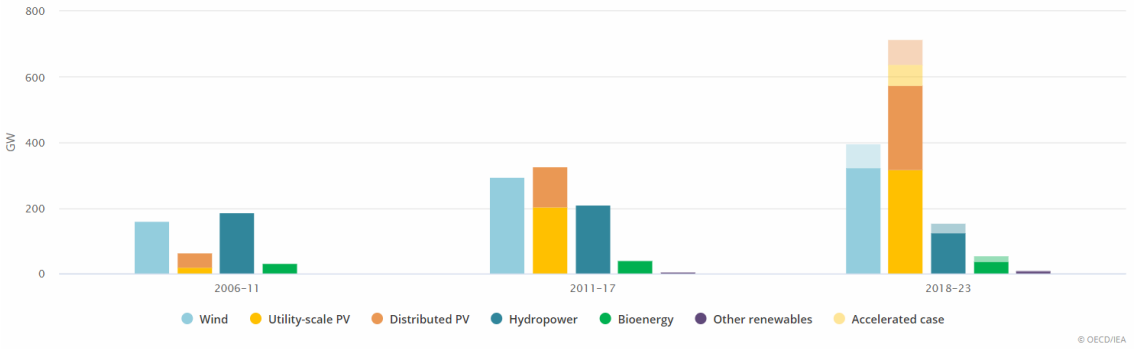

Figure 1.3: Net renewable capacity additions, main and accelerated case, 2006-2023 [6]

Because of their ability to supply energy independently from the grid and their low environmental footprint, renewable energies have become an attractive solution to rural areas.

1.3 Micro-grids as a solution

The inhabitants of rural areas have three main different ways to gain access to electricity. These can be classified into centralized and decentralized systems. The first method is by expanding the main grid and thus becoming a centralized system. The decentralized methods are micro-grids and off-grid systems. Off-grid systems consists of systems that are not connected to any kind of grid. Examples of these kind of systems are household photo-voltaic (PV) panels or diesel generators. Both micro-grids and off-grid systems provide an alternative way to develop rural areas. According to [4], it has been determined that in rural areas the decentralized approaches are the most cost effective solutions for more than two-thirds of those who gain access to the electricity.

It is important to compare the available methods to see why would one prefer a micro-grid over the other methods. Figure 1.4 illustrates the different types of technologies that can be accessed depending on which type of electrification method is used. It can be seen that micro-grids have the capability to provide access to the same technologies the main grid would. Meanwhile, off-grid systems are not able to provide cooling and large appliances, and they are also limited in the area of industry and telecommunications. Compared to the off-grid systems, Micro-grids have two main advantages [7]:

- Micro-grids are able to use electricity more efficiently as they can connect several users
- Micro-grids can accommodate large generation units which allows them to supply larger loads

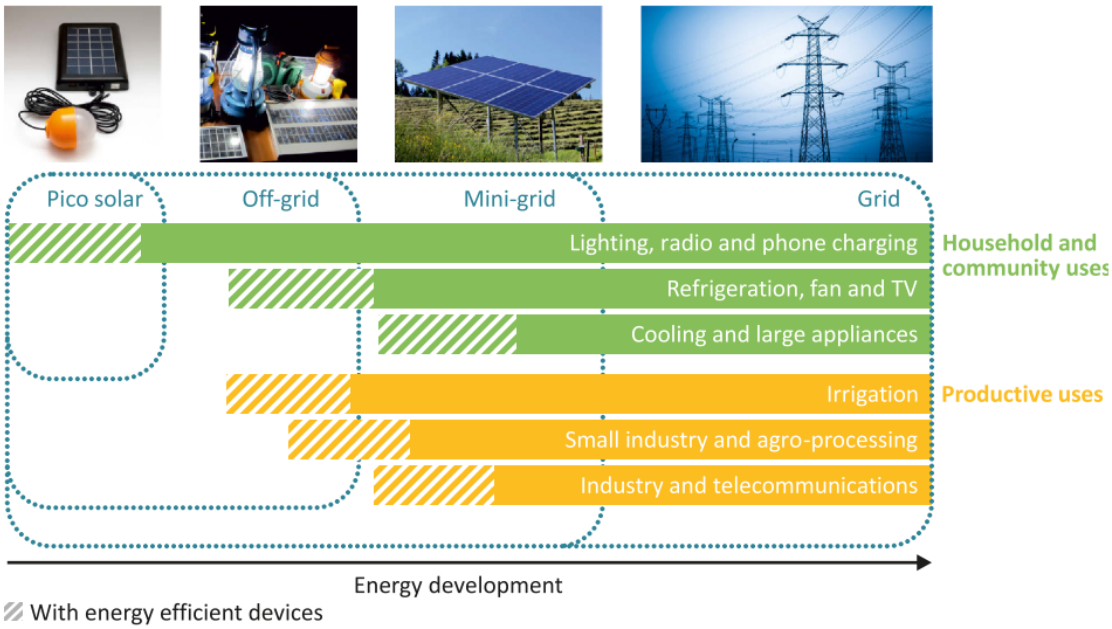

Figure 1.4: Electricity access and illustrative technology options [4]

It is worth pointing out that micro-grids do not only have potential in terms of efficiency and capabilities, but in economic terms as well. In the world energy outlook 2007, a study was made in how to provide electricity to all by the year 2030 in accordance with the SDG7 (sustainable Development Goal 7) in the most economical manner. The resulting best option is using three different connections which are through the grid, through micro-grids, and through off-grid sources. However, the majority of the people who will gain access will do so through micro-grids. The results of the study are shown in figure 1.5. It is also worth considering that micro-grids have two additional beneficial characteristics. They can increase their capacity as it is needed, and they connect to the grid when such option becomes available.

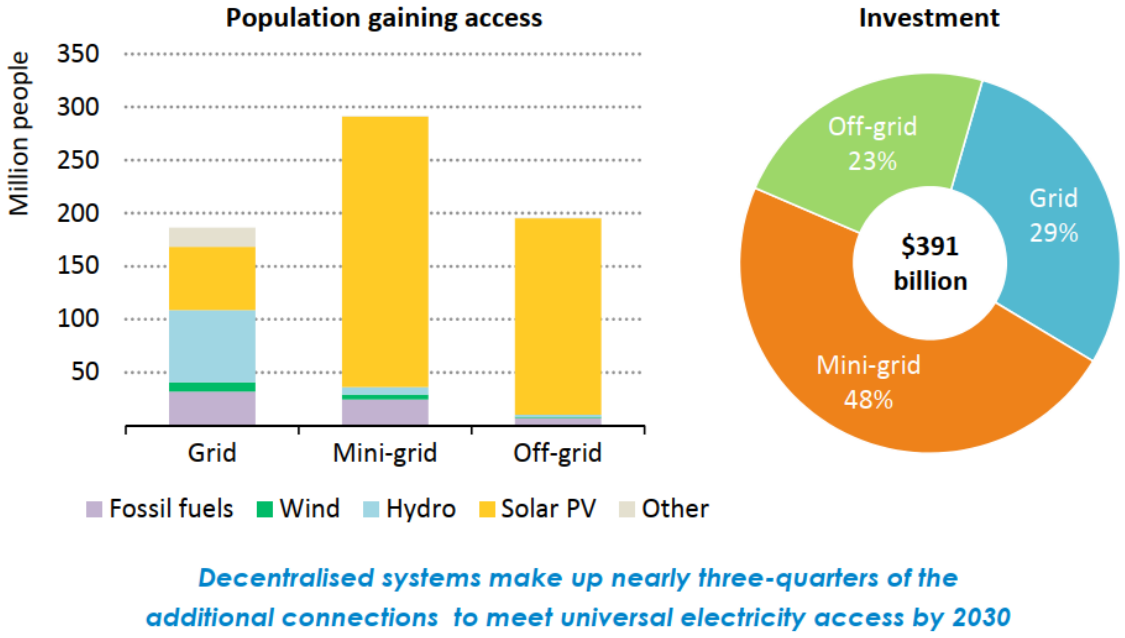

Figure 1.5: Additional population gaining access and additional investment in the Energy for All Case relative to the New Policies Scenario, 2017-2030 [4]

In 2019 the Energy Sector Management Assistance Program (ESMAP) made a study about the future of micro-grids for rural electrification. In 2019, 47 million people had access to the electricity through micro-grids. In order to achieve the SGD7 goals by the year 2030, 490 million people will be served through micro-grids [8]. The updated data shows that more people are expected to connect through the micro-grids than the almost 300 million initially calculated.

Chapter 2

Micro-grids

Micro-grids are local grids that are comprised of distributed generators (DG), energy storage systems (ESS) that feed loads, and also have some telecommunication elements. They can operate connected to a grid or autonomously which is what is often referred to as islanded mode [9]. The general structure of a micro-grid is given in figure 2.1. Micro-grids due to their size usually use low voltage buses. The different generators and loads attach to a main single bus that is referred to as the point of common coupling (PCC). It is also at this point that the micro-grid is connected to the main grid through substations or circuit breakers.We can additionally define some characteristics of a micro-grid [1]:

- Ease of integration of new resources
- Ease of scaling up or down the size
- Equitable role for each resource in determining the operation of the micro-grid

For the context of electrification of rural areas these are great characteristics. It can be expected that as the area develops, the loads that they would need to cover will increase. Therefore, being able to add resources and scale its size up makes micro-grids a viable long term solution for such communities.

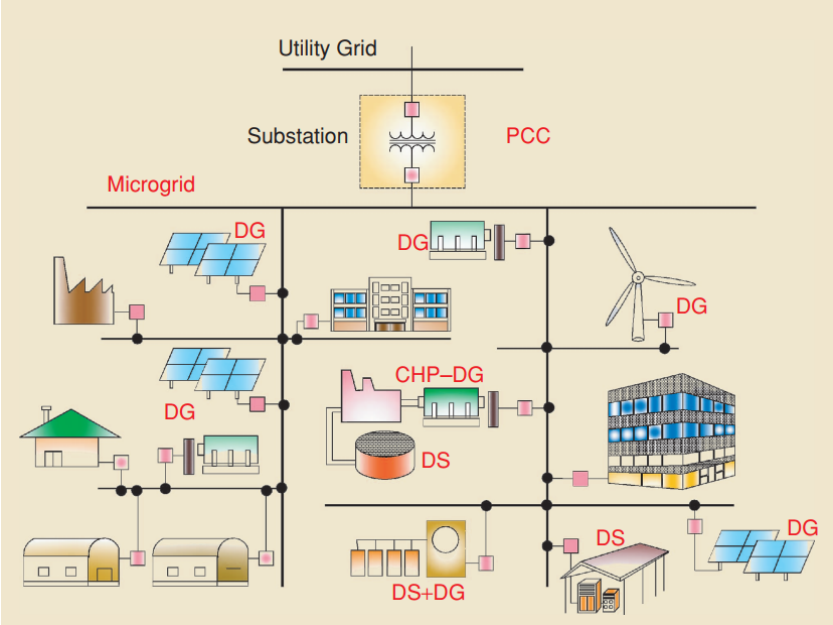

Figure 2.1: Typical microgrid structure including distributed loads, generators, and storage units serviced by a distribution system [10]

Other than being classified as grid-connected or islanded, micro-grids can also be classified based on the type of voltage adopted on its buses. We can identify three types: AC, DC ,and Hybrid micro-grids. Studies have been done in order to identify which type is more suitable for which occasion. In [11] it is suggested that most determining factor could be the ratio of DC loads. If there are more DC loads than AC loads a DC micro-grid can provide economical advantages over AC micro-grids. The different advantages posed by DC and hybrid micro-grids are still being studied. In this master thesis only 3 phase AC micro-grids will be considered.

The defining characteristic of AC micro-grids is that their behaviour is analogous to that of a large-scale grid. As a consequence, similar control methods and conventional devices can be used. Figure 2.2 shows an example of a basic AC micro-grid structure. One key element in the structure of the micro-grid is the use of converters. Distributed generators such as PV or Energy storage systems output their power in DC. In order to connect to the main AC bus the output has to go through an DC/AC converter. In the case of wind turbines and micro-turbines their power output is already in AC, but it might not be the same frequency or voltage as the bus. Therefore they must first convert from AC to DC and then DC back to AC.

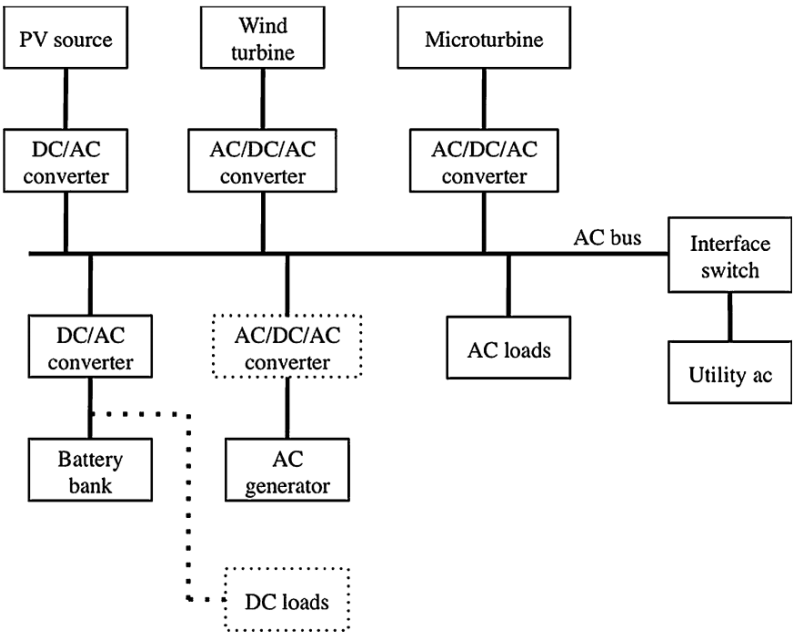

Figure 2.2: Simplified schematic illustration of an AC microgrid [1]

2.1 Control levels

As the implementation of micro-grid systems is becoming more widespread, the need for the development of standards has increased. To cover this need the standard ISO-95 was adopted. This is a multi level hierarchical control [12]. The levels are distributed as follows [12], [13]:

- Level 0 (Innerloop control): Deals with the regulation of the operation of each module. Mainly the control of the output voltage and current.
- Level 1 (Local control loop): Deals with emulating physical behaviors that makes the system stable and more damped. Usually this is achieved through droop controllers.
- Level 2 (Secondary control loop): This level is controlled by the micro-grid central controller (MGCC). It ensures that frequency and voltage of the grid are at the correct values. It also manages load shaving, and disconnection of micro-grid from other networks
- Level 3 (Tertiary control): Deals with the power flow between the micro-grid, the main grid, and the energy market.

For islanded micro-grids the third level is not a applicable as there is no existing connection to the main grid. This thesis will focus on the local control loop which corresponds to level 1 and the inner control loop corresponding to level 0. In chapter 3 different control methods used in level 1 will be explored.

2.2 Grid forming and grid following units

As discussed earlier, distributed generators need to use power electronics to adapt their output voltage and frequency to that of the micro-grid. Nevertheless, it is also important to discuss how the values of the grid are set. In traditional grids synchronous generators perform this role, but such generators are not common in micro-grids. Thus, the responsibility for setting such quantities falls on the DGs themselves. Depending on the role they play the DGs can be classified as [14]:

- Grid-forming unit: It balances the the power of generator in order to set the grid voltage and frequency of the grid. This type of unit can be seen as an ideal ac voltage source.
- Grid-feeding unit: Its main objective is to feed power into the grid. This type of unit can be seen as an ideal current source. It can not operate by itself in an islanded micro-grid as it needs a grid-forming unit to set the voltage and frequency of the grid.
- Grid-supporting unit: It can participate in the regulation of the grid voltage and frequency while supplying active and reactive power at the same time. This type of converter can be operated as either an ideal ac current source or an ideal ac voltage source.

Figure 2.3 shows the simplified representation for each type of DG unit. Figure 2.3 a) represents a grid-forming unit. ω^* and E^* represent the reference voltage amplitude and reference frequency to be set by the DG. The control block C_v takes as inputs ω^* and E^* in order to give the reference voltage V^*. Figure 2.3 b) represents a grid-feeding unit. In this case P^* and Q^* give the reference active and reactive power to be delivered. C_p acts as the control block that gives the corresponding reference current i^*. Finally figure 2.3 c) and d) represent grid-supporting units as a current source or a voltage source respectively. For the grid-supporting unit acting as a current source the reference angular frequency ω^* and the reference voltage amplitude E^* go through their respective controllers C_ω and C_E. The output of C_ω is compared against P^*, and the output of C_E is compared against Q^*. Through this process, the new references for the active power P^{**} and reactive power Q^{**} are generated. These two quantities are inputted into the power controller C_P in order to give the reference current i^*. Once P^{**} and $Q^{*}*$ are calculated the behaviour of the system is analogous to a grid-feeding DG. In the case of the grid-supporting units acting as voltage sources, P^* and Q^* go through their respective controllers C_P and C_Q. The output of C_P is compared with w^* to give the new reference w^{**}. Equally, the output of C_Q is compared against E^* to produce the new reference E^{**}. The new references are fed to the voltage controller C_v replicating the process of a grid-forming rectifier.

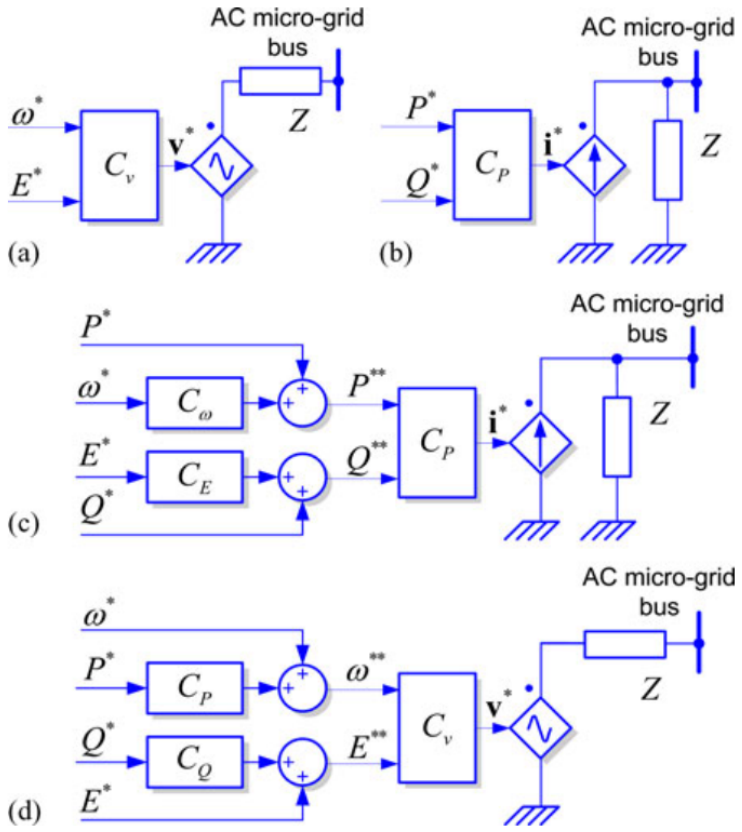

Figure 2.3: Simplified representation of the different types of DG units [14]

In this section, two different control approaches that use different types of units are compared. The first one is the master/slave control approach. In this control strategy there is a master unit which is a grid forming unit, and the other units are either grid following or grid supporting units. The master unit is in charge of setting the grid voltage and frequency and of specifying the reference current to the other units. Meanwhile, the grid following units follow the reference current specified for each one of them.

The second approach is one based on the traditional droop control. The behaviour of synchronous generators on the grid is a product of the inertia of the motors that cause them to slow down when extracted power is larger than its input mechanical power. This results in a decrease of the phase and voltage [15]. This control strategy is used on the DGs in order to mimic the previously explained behaviour of synchronous generators. This type of control can be implemented with grid supporting units. However, if the grid-supporting units are implemented as an ideal AC current source they need at least one grid forming unit in order to operate. On the other hand, when grid-supporting units are implemented as ideal AC voltage sources, a grid-forming unit is not needed[14]. This is because grid-supporting units acting as a voltage source can participate in the grid voltage and frequency regulation while supplying active and reactive power. This type of units are interfaced by Voltage source inverters (VSI) that allows them to build the voltage as its control specifies it. If all the units on the grid act as grid-supporting voltage sources, it will lead to a grid where all the units contribute to the regulation of voltage and frequency.

At the same time this system automatically enables load sharing between the DGs [16]. This eliminates the need of having grid forming and grid following devices, and thus the master/slave operation is not needed at all.

The main advantage of the droop control approach is that it does not have high communication requirements as only the reference values for voltage and frequency need to be provided. Table 2.1 provides a comparison between both approaches.

	Master/Slave Control	**Droop Control**
Advantages	- Simple control algorithm in controllers	- Simple expansion of the system - Increased redundancy as there is no need to rely on control bus system - A simple bus is sufficient for optimization - Simplified supervisory control
Disadvantages	- High cost of busses and their cabling - Difficult expansion of the system - Supervisory control required	- More complex control tasks in the components

Table 2.1: Master/slave control and droop control comparison [17]

By comparing which system would be better for the purpose of rural electrification, it can be seen that the Droop control approach posses more advantages. The high cost of the busses and cabling could become an impediment for rural installations. Even if the cost of the installations is ignored, there is another important disadvantage which is that the expansion of the system is difficulty. It would be expected that the community will grow as it develops specially after obtaining electricity. Therefore, this drawback has a significant weight in rural applications. The increased reliability of the droop control is also a desirable characteristic. This increased reliability comes mainly from the redundancy attributed to fact that no communication is needed among the generators. Therefore, the control will not be affected by any type of communication delays or interruptions. As discussed in chapter 1, rural areas are often geographically isolated. Therefore, technical assistance may not have the required response time. This is why having a robust and simple control is beneficial for the system.

Chapter 3

Local control methods

As discussed in section 2.1 the control of micro-grids can be divided into levels. This thesis focuses mainly in level 1 which is the local control loop and level 0 which is needed in order to achieve this. The goal of level 1 is to provide a control for the active and reactive power such that the micro-grid is able to emulate the physical behaviour of the normal grid. Although there are control methods for grid forming and grid following units, this section will focus only on the grid-supporting units acting as voltage sources as they have the advantages described in the previous section. Figure 3.1 shows some of the existing control strategies with or without communication. This chapter will focus mainly on two different methods that do not need communication. These are the P.V/Q.F control and P.F/Q.V control.

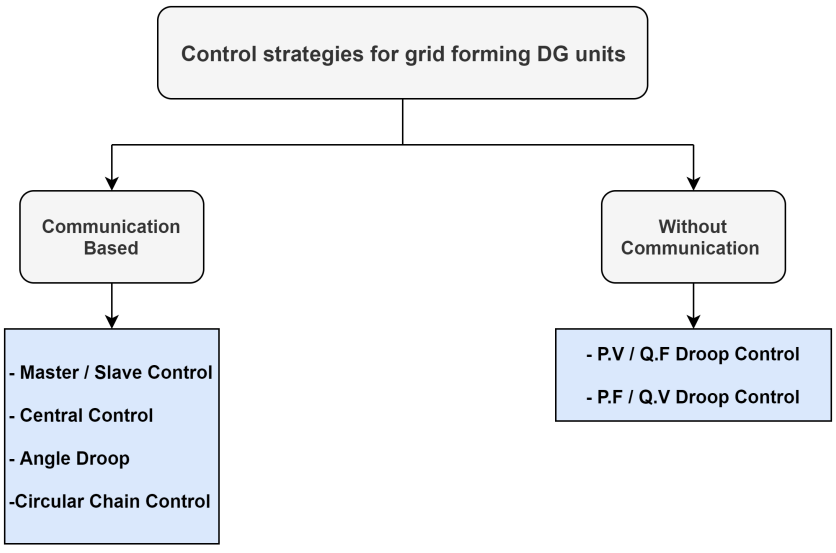

Figure 3.1: Grid forming DG control strategies [18]

3.1 P.F / Q.V droop control

This type of droop control is also called the "conventional" droop control. It is the one used in standard grids. Its equations can be derived from the the circuit shown in figure 3.2. Figure 3.2 illustrates V_A which is an ideal voltage source connected through a line to V_B which represents the grid. When we consider the exchange in active and reactive power in this circuit, the exchange can be expressed as developed in [14]:

$$P_A = \frac{V_A}{R^2 + X^2} \left[R(V_A - V_B cos\delta) + X V_B sin\delta \right] \tag{3.1}$$

$$Q_A = \frac{V_A}{R^2 + X^2} \left[-R V_B sin\delta + X(V_A - V_B cos\delta) \right] \tag{3.2}$$

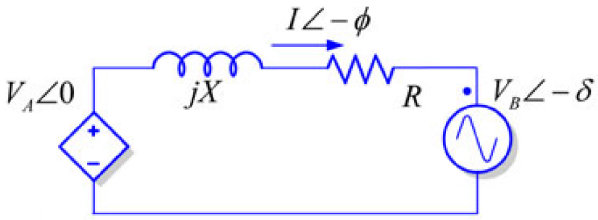

Figure 3.2: Simplified modeling of power converter connection to a distribution network [14]

If the resistive part is neglected, then one simplify the previous equations. Thus, it is obtained:

$$P = \frac{V_A V_B}{X} sin\delta \tag{3.3}$$

$$Q = \frac{V_A^2}{X} - \frac{V_A V_B}{X} cos\delta \tag{3.4}$$

Since the power angle δ is small, it is possible to further simplify these two equations into:

$$P_A \approx \frac{V_A V_B}{X} \delta \Rightarrow \delta \approx \frac{X P_A}{V_A V_B} \tag{3.5}$$

$$Q_A \approx \frac{(V_A - V_B) V_A}{X} \Rightarrow V_A - V_B \approx \frac{X Q_A}{V_A} \tag{3.6}$$

Therefore based on equations 3.5 and 3.6, it can be seen that there is a link between the power angle and the active power, and there is a link as well between the reactive power and the difference between voltages. It is from these observations that it is claimed that if one can control the active and reactive power output, it is possible to control the phase angle and voltage V_A. However in a micro-grid, each DG does not know what is the phase of the other DGs. Therefore, instead of using the power angle, each DG uses the frequency of the grid as it is the same for all the DGs on the grid [19]. This is possible if we consider the relationship between power angle and the frequency:

$$f = \frac{\omega_N}{2\pi} = \frac{\partial \delta}{\partial t} \tag{3.7}$$

By taking into account the relationship between the variables it is possible to adjust one in function of the other. For example, a change in frequency Δf will correspond to a change in active power ΔP. In this case the delta is defined by the variation of the quantity with respect to its nominal value. How much should the active power respond to a Δf is defined by a slope. This slope is described by the droop coefficient. Such relationship is the one described by equations 3.8 and 3.9

$$f - f_n = -K_p(P - P_n) \tag{3.8}$$

$$V - V_n = -K_q(Q - Q_n) \tag{3.9}$$

In these equations f_n, P_n, V_n, and Q_n represent the nominal values. K_p and K_q are the droop coefficients that define the characteristic slope of the droop control. An example of the slopes that define the droop characteristics is shown in figure 3.3. Finally, figure 3.4 shows a block diagram implementation of this control.

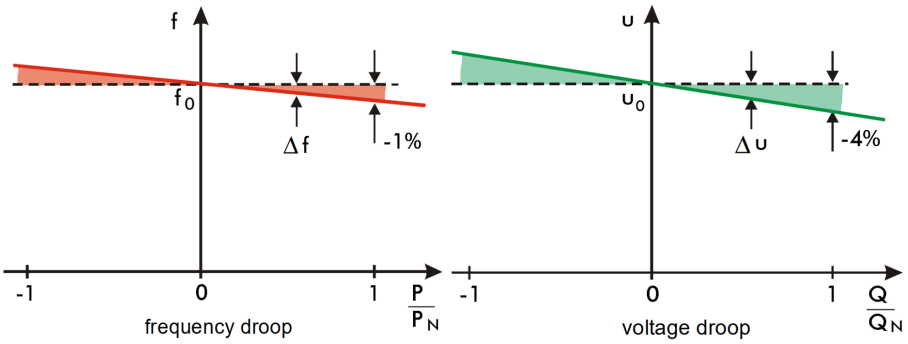

Figure 3.3: P.F / Q.V Droop characteristics [17]

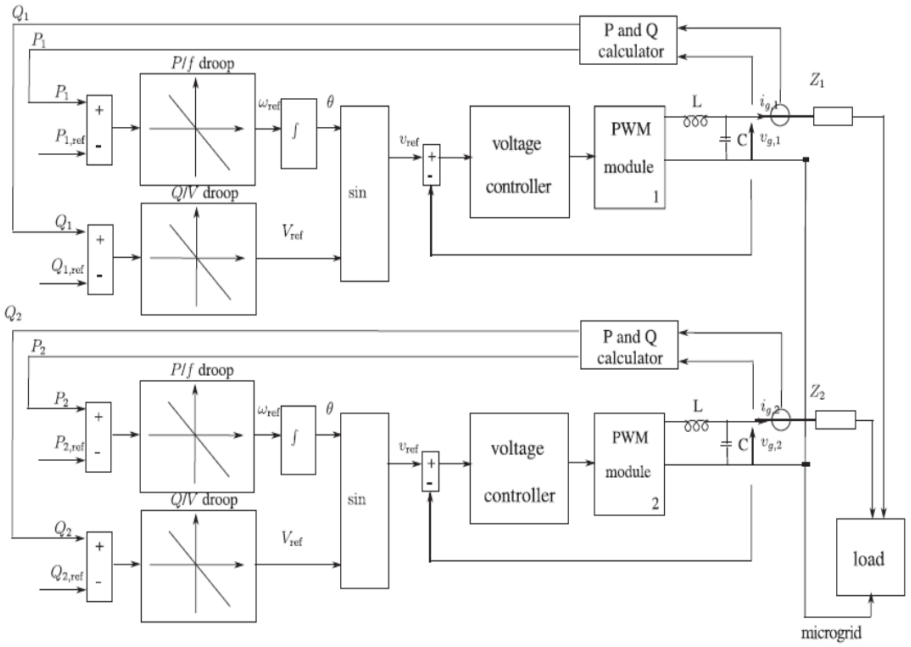

Figure 3.4: P.F / Q.V Droop control block diagram [18]

3.2 P.V / Q.F droop control

In the case of micro-grids, these are composed mostly of low voltage lines. These lines have the characteristic that they are mostly resistive ($X << R$). This results in having sightly different equations for the reactive and active power flow. If in equations 3.1 and 3.2 the reactance is neglected instead of the resistance, the found equations in a low voltage line are:

$$P \approx \frac{V_A^2}{R} - \frac{V_A V_B}{R} cos\delta \tag{3.10}$$

$$Q_A \approx -\frac{V_A V_B}{R} sin\delta \tag{3.11}$$

If it is again considered that the angle δ is small, one can reduce the previous equations into equation 3.12 and equation 3.13. By looking at the relationship between these two equations the power circle diagram shown in figure 3.5 can be obtained. The system would operate on the left side of the power circle which corresponds to δ values from $-\pi/2$ to $\pi/2$.

$$P \approx \frac{(V_A - V_B)V_A}{R} \Rightarrow V_A - V_B \approx \frac{RP_A}{V_A} \tag{3.12}$$

$$Q \approx -\frac{V_A V_B}{R}\delta \Rightarrow \delta \approx -\frac{RQ_A}{V_A V_B} \tag{3.13}$$

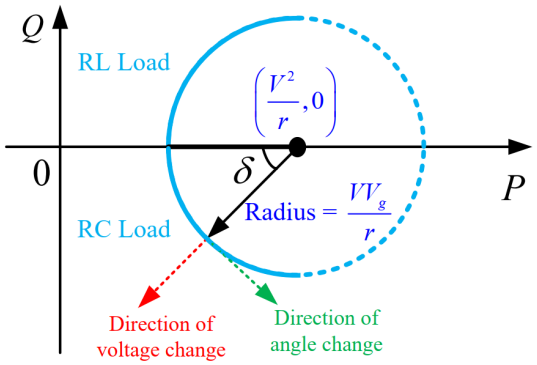

Figure 3.5: Power circle diagram in a resistive grid [20]

From the previous equations, it can be seen that the formulas for P and Q are the inverse than that of the conventional droop control. For this reason this control can also be referred to as "opposite" droops. Once again the variables can be linked to each other by the slope defined with the droop coefficient. The obtained opposite droop equations are shown in equation 3.14 and 3.15. Meanwhile, figure 3.6 shows the implementation of such droop control using block diagrams.

$$V - V_n = -K_p(P - P_n) \tag{3.14}$$

$$f - f_n = K_q(Q - Q_n) \tag{3.15}$$

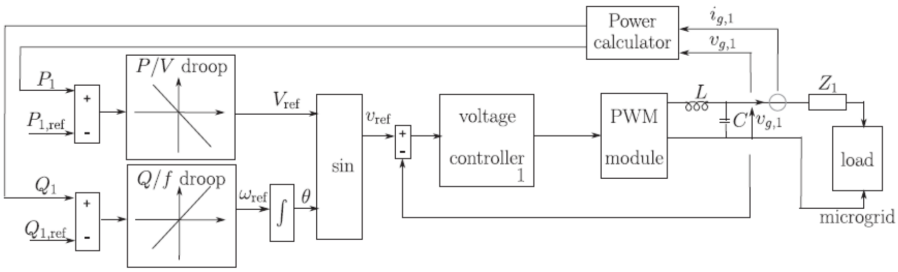

Figure 3.6: P.V / Q.F Droop control block diagram [18]

3.3 P.V / Q.F droop control On resistive lines

As shown in the previous section, if the lines are mainly resisitive this leads to different active and reactive power equations. The active power depends on ΔV and the reactive power on $\Delta\delta$. Thus, if the traditional droop control is used on such lines, it can produce undesired effects. The result would be a system where increasing the active power results in decreasing the reactive power, but increasing the reactive power results in increasing the active power [21]. This is due to the coupling between the droop controls which is described in figure 3.7. On the first diagram when a change in power occurs this causes a change in the frequency due to the droop control. The frequency is related to the power angle δ. Thus ΔP causes a $\Delta\delta$. The $\Delta\delta$ causes a ΔQ which due to its droop control causes a ΔV. Since in a resistive grid the active power depends on ΔV, this ΔV leads again to the ΔP. As shown in figure 3.7 on the second diagram, a similar chain happens when one starts with a ΔQ. It is also thus shown that $\Delta\delta$ indirectly controls ΔP, and that ΔV indirectly controls ΔQ

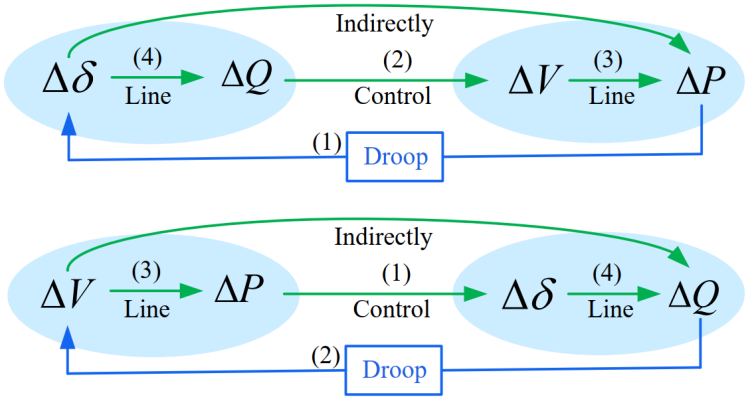

Figure 3.7: Droop control coupling relationship [20]

Thus a change in power will lead to an undesired change in the reactive power. While a change in reactive power also changes the active power, this effect is not as noticeable. This is due to the fact that as the voltage V_A changes, V_B is also changed. This results in a ΔV that is only sightly changed. Thus, the effect of a ΔQ on the active power is minimized.

Chapter 4

Modeling

In this chapter, The different elements that constitute a DG are shown. During the first part of the chapter how these different parts were modeled is shown. The model is then evaluated on the test grid to be described in this chapter. With this test grid the traditional and opposite droop control methods are evaluated through different tests. The model described in this chapter was implemented on MATLAB/Simulink. The different electrical and power system components were represented using the Simscape library.

4.1 Distributed generators

As previously mentioned the Distributed generators are the main sources of energy in the micro-grid. They consists of renewable energies coupled with power electronics. The main role of the inverter will be to adapt the output voltage and frequency according to the desired grid values. In this case, inverters consisting of diodes and Isolated Gate Bipolar Transistors (IGBT) were selected. The inverters are connected to PV array which acts as a power source. The power of each inverter is defined by the capacity of the PV array. These are considered to be operating under a constant irradiance of 1 kW per meter squared and a temperature of 25 degrees Celsius. The power and output voltage is defined by the number of series connected modules, and the number of parallel strings. The PV arrays are placed in parallel with a resistor in series with a capacitor that interface the inverter. This capacitor acts as the DC link. The DC link capacitor has two main roles. The first one is to provide a low impedance path for the ripple currents from the inverter. The second one is to reduce the leakage inductance of the inverter so to reduce the effects of the voltage spikes caused when the devices are switched on and off [22]. Figure 4.1 shows the general structure of the distributed generators used in the simulations. The inverter is controlled through Pulse width modulation (PWM) signals generated from the reference voltage. The reference in voltage in exchange is set by the droop control and the innerloop control. The output lines of the inverter are followed by an LCL filter.

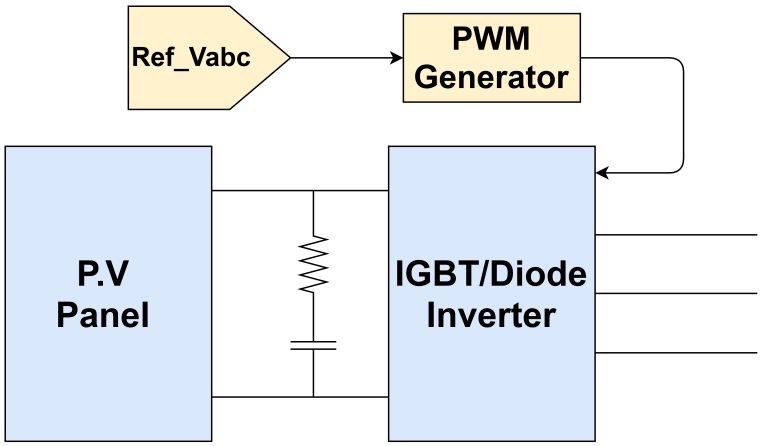

Figure 4.1: Distributed generator structure

The coupled system of the PV panel and the VSI has a limitation in terms of active and reactive power output. The limit for the active power is the maximum active power that the PV can produce. The VSI can not produce active power so the responsibility relies on the PV panel. In terms of reactive power the situation is reversed. The PV panel can only generate active power and thus the responsibility to manage the reactive power lies on the VSI. The voltage and current limits of the VSI will be the main limiting factor for the reactive power generation. The voltage limit, current limit, and power limit curves can be used to obtained the operational area. This area and its limits are shown in figure 4.2. For this simulation the active power limits are present due to the PV panel having a limited active power output. However, the VSI model used is ideal and does not have a specific limitations in place.

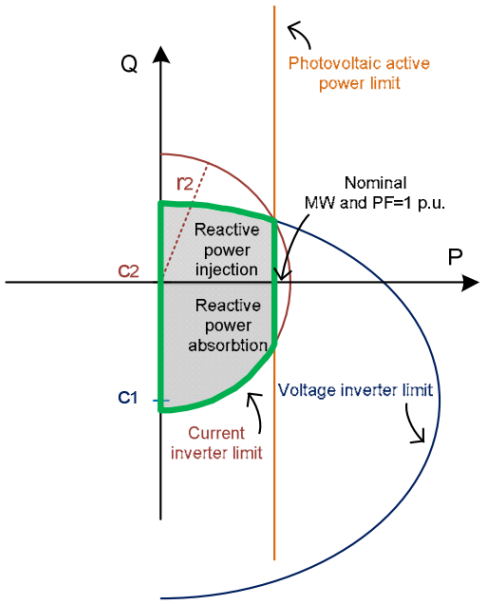

Figure 4.2: Active and reactive power limitations on a PV panel interfaced by a VSI [23]

It is worth pointing out that the depiction in figure 4.1 can not be applied as it is in a realistic scenario. As mentioned before for this simulation it has been assumed that the power of the PV panel is constant. This is not the case in real applications as the power will depend on the position of the sun and in the control method applied to the PV panel. Energy storage systems such as batteries are usually placed in order to compensate the fluctuations of power of the PV panel. This ensures that the DG will be able to supply its rated power at all time.

4.1.1 LCL output filter

Because of the adaptive role that the inverter plays, PWM is often used in order to regulate the values of the voltage. The switching involved with PWM introduces switching harmonics and their multiples into the system [24]. It is because of this that inverters are often followed by a filter. There are L, LC, and LCL filters. The LCL filters provide different advantages with respect to the others. The LCL filter has better attenuation and dynamic characteristics. Additionally, it has better decoupling between the impedances of the filter and the grid. Finally, it provides lower current ripple across the grid inductor [25]. However, the filter is also susceptible to resonance problems. A resistor is added in series with the capacitance in order to prevent resonance and reduce the ripple. It is worth noticing that this will increase the heat losses in the system and reduce the efficiency of the filter. An additional measure taken in order to avoid resonance problems is to place a constraint on the resonance frequency of the filter. The resonance frequency obtained should be higher than ten times the grid frequency, but lower than half the switching frequency [24].

$$10f_g < f_{res} < 0.5f_{sw} \tag{4.1}$$

Figure 4.3 shows the schematic of the LCL filter connected to each output phase of the inverters. l_i is the inverter side inductance. Rd is the damping resistance. C_f is the filter capacitance. Finally, l_g is the grid side inductance.

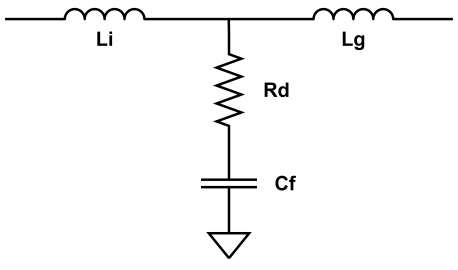

Figure 4.3: LCL filter schematic

4.1.2 Droop control

The droop control is a mechanism in which a reference voltage and frequency are set. The generators or inverters in this case modify their output voltage and frequency as a function of their power output. This is done in order to simulate the behaviour or response of synchronous generators [26]. The voltage and current at the LCL filter are used to calculate the active and reactive power. These powers serve as the input of the droop control. The type of droop controls implemented are the P.F / Q.V droop which was discussed in section 3.1 and the P.V / Q.F droop from section 3.2. The droop control is often followed by a cascade controller which consists of PI controllers. The droop control is referred to as the primary control or external power control loop. It is tasked with controlling the reference voltage and frequency by using droop controls. Meanwhile, the cascade controller is known as the innerloop which is tasked with regulating the three phase inner voltage [27]. The output of the innerloop serves as the reference voltage used to generate the PWM signal the guides the operation of the VSI. In the hierarchical control scheme the innerloop corresponds to the level 0. Figure 4.4 shows the general schematic of the previously mentioned controllers. In figure 4.4 the droop coefficients are represented by n_d and m_d. n_d corresponds to the droop coefficient K_q and m_d corresponds to the coefficient K_p

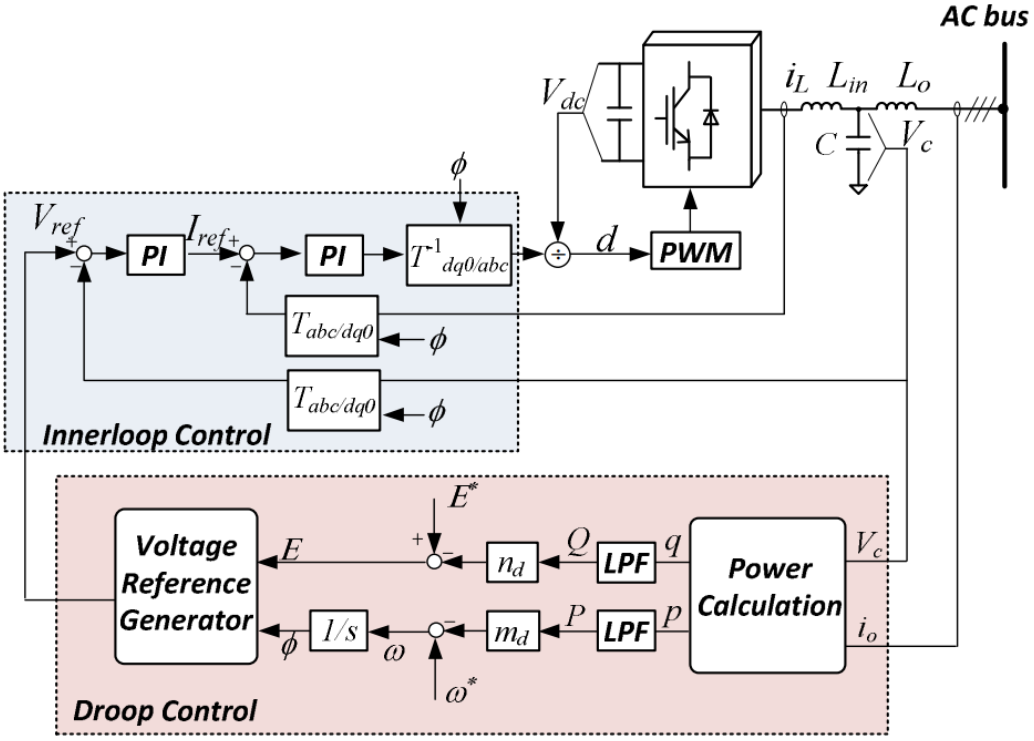

Figure 4.4: Distributed Generator control loop schematic [28]

There are different variations to the inner and primary control loop of the droop control. For example the innerloop control can also be one such that it includes voltage control, but no current control loop. Such an example can be seen in [29]. It can also be used with or without decoupling terms as shown in [27] or [30].

The droop/primary control used in the P.F/Q.V control is shown in figure 4.5. The voltage before the grid inductor l_g and the current before the inverter inductor l_i are measured and transformed into their dq0 components. The dq0 components represent the direct, quadrature, and zero components of a synchronous reference rotating frame. When working on the abc frame the quantities such as current and voltage are oscillating as a function of the angle θ. The dq0 transforms the abc variables into a synchronous rotating frame which causes the variables to be seen as steady values or dc signals. These DC equivalent signals will still change and react to perturbations to the system. The transformation from abc to dq0 is implemented in Simulink as shown in equation 4.2. The inverse transformation from dq0 to abc is implemented as shown in equation 4.3.

$$\begin{bmatrix} u_d \\ u_q \\ u_0 \end{bmatrix} = \frac{3}{2} \begin{bmatrix} cos(\omega t) & cos(\omega t - \frac{2\pi}{3}) & cos(\omega t + \frac{2\pi}{3}) \\ -sin(\omega t) & -sin(\omega t - \frac{2\pi}{3}) & -sin(\omega t + \frac{2\pi}{3}) \\ \frac{1}{2} & \frac{1}{2} & \frac{1}{2} \end{bmatrix} \begin{bmatrix} u_a \\ u_b \\ u_c \end{bmatrix} \tag{4.2}$$

$$\begin{bmatrix} u_a \\ u_b \\ u_c \end{bmatrix} = \begin{bmatrix} cos(\omega t) & -sin(\omega t) & 1 \\ cos(\omega t - \frac{2\pi}{3}) & -sin(\omega t - \frac{2\pi}{3}) & 1 \\ cos(\omega t + \frac{2\pi}{3}) & -sin(\omega t + \frac{2\pi}{3}) & 1 \end{bmatrix} \begin{bmatrix} u_d \\ u_q \\ u_0 \end{bmatrix} \tag{4.3}$$

The dq0 components are used to calculate the active and reactive power. These powers are both passed through a low pass filter. The low pass filter is needed because we are dealing with a non ideal Ac source and therefore its signals contain harmonics and noise. Because of these non idealities, the calculated active and reactive powers are not constant and cause fluctuations in the generated reference voltage and frequency. If let unattended the oscillations can feedback into the system and amplify the distortion of the generated power. The role of the low pass filter is to smooth such signals so to reduce the harmonics and noises [31].

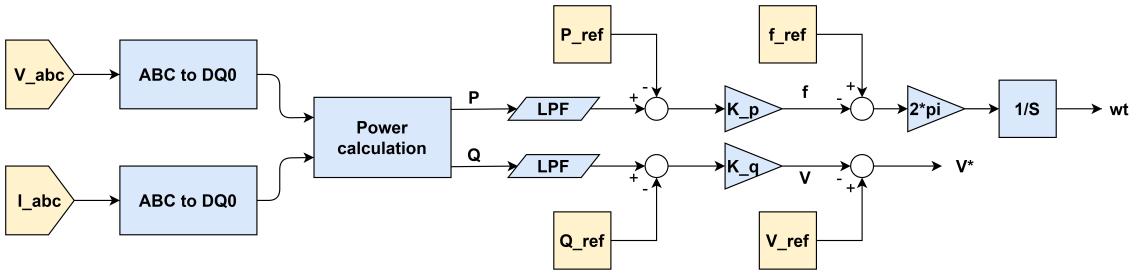

Figure 4.5: Implemented P.F/Q.V droop control loop schematic

The filtered values are compared to the reference power values, which can also be referred to as the set-point. This difference is then multiplied by the droop coefficients. The coefficients are chosen so that each distributed generator can contribute to the total power requested in proportion to its available capacity. According to [15] these coefficients can be defined for each DG as shown in equation 4.4 and equation 4.5. However, in the literature there are sightly different approaches to calculating the droop coefficients as it is done in [28].

$$K_p = \frac{\omega_{ref} - \omega_{min}}{P_{ref} - P_{max}} < 0 \tag{4.4}$$

$$K_q = \frac{V_{ref} - V_{min}}{Q_{ref} - Q_{max}} < 0 \tag{4.5}$$

According to [27] the acceptable voltage and frequency deviations can be taken from the Institute of Electrical and Electronics Engineers (IEEE) 1547 standard. This is the "standard for IEEE Standard for Interconnection and Interoperability of Distributed Energy Resources with Associated Electric Power Systems Interfaces". Based on this it is recommended to have a maximal deviation from the reference value of 5% for the voltage and 1.4% for the frequency.

The resulting product of the droop coefficient and the difference between P and P_{ref} or Q and Q_{ref} is then subtracted from the reference frequency and reference voltage value. The resulting frequency is then multiplied by 2π and integrated resulting in wt. This wt is used in the $dq0$ transformations needed for the calculation of powers and for the innerloop control.

In the case of the P.V/Q.F droop control, the schematic is modified as seen in figure 4.6. In this graph it is shown that the active power is related to the voltage and the reactive power to the frequency. It is also important to remember that the droop coefficients are calculated differently as ΔV is related to K_p, and $\Delta\omega$ is related to K_q. This is shown in equations 4.6 and 4.7. Other than these changes the procedure followed is the same as for the P.F/Q.V control.

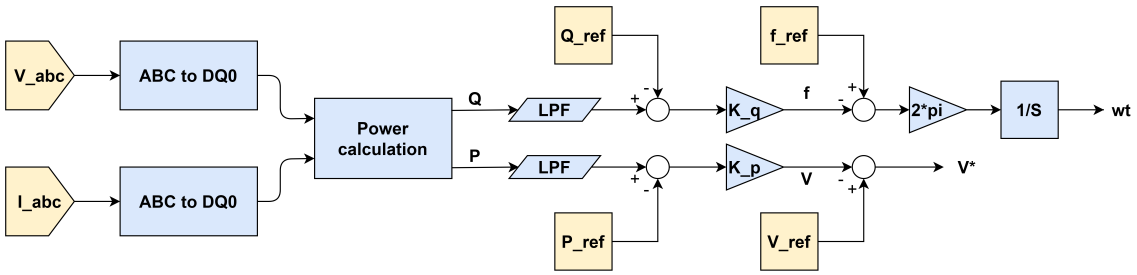

Figure 4.6: Implemented P.V/Q.F droop control loop schematic

$$K_p = -\frac{V_{ref} - V_{min}}{P_{ref} - P_{max}} < 0 \tag{4.6}$$

$$K_q = \frac{\omega_{ref} - \omega_{min}}{Q_{ref} - Q_{max}} < 0 \tag{4.7}$$

The innerloop control is done in the $dq0$ reference frame. For the voltage control, the calculated reference voltage V^* is taken as the d component and its compared with the voltage V_d measured before the output inductor l_g. Their difference is then feed into the PI controller. The reference q voltage value is set to zero and compared with the voltage V_q repeating the process mentioned before. The reference q voltage is set to zero in order to have only positive sequence components in the abc reference frame [30]. The resulting outputs are then compared to the d and q components of i_i which is the current flowing through the inductance l_i. The dq components are then transformed into the abc reference frame and act as the reference voltage fed into the PWM Generator. The current control is used to adjust the current so that i_i can charge the filter capacitor C_f to a voltage level similar to the one provided as a reference [14]. The values for the PI controllers have to be chosen carefully. A wrong set of values will cause the system to be unstable and to have large fluctuations. The values have to be chosen so that the response has an acceptable speed, but avoiding having a strong overshooting. Choosing a good set of values will also limit the ripple after a transient.

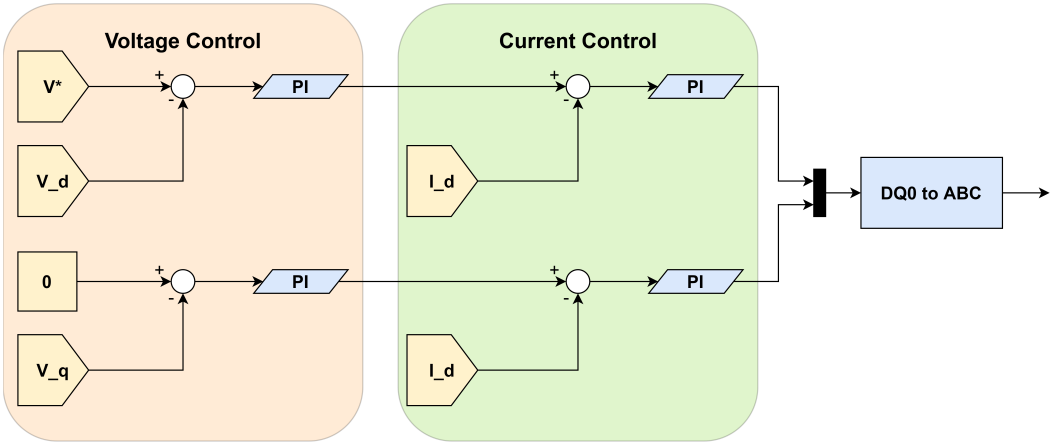

Figure 4.7: Innerloop control

4.2 Line characteristics

Micro-grids for rural areas such as the ones proposed cover relatively small areas of few kilometers. In this case a micro-grid with lines of length equal or less to $2km$ is studied. Due to the size of areas covered only low voltage distribution lines are used. Table 4.1 shows the typical line parameters. It can be observed that low voltage lines have a much higher resistive component when compared to medium and high voltage lines. On the

other hand, the inductive component of low voltage lines is smaller than the other types of lines. Thus, it can be said that the low voltage lines are mainly resistive as shown by the ratio R'/X'.

Type of line	**R'** Ω/km	**X'** Ω/km	I_N A	$\frac{R'}{X'}$
Low voltage line	0.642	0.083	142	7.7
Medium voltage line	0.161	0.190	396	0.85
High voltage line	0.06	0.191	580	0.31

Table 4.1: Typical line parameters [32]

4.3 Virtual impedance

Due to the differences in the lines, there is a mismatch in the impedance that causes problems in terms of reactive power sharing. Furthermore, a high R/X ratio can lead to coupling and dynamic instability in the power control when using the traditional droop control [27]. The virtual impedance helps fix the output impedance which in turn affects the output active and reactive power angle and amplitude [9].

The impedance can be applied physically, but if it is done virtually at the innerloop level, it is possible to obtain equally effective results. Additionally, due to the fact that it is virtual there are no dissipation losses. Another advantage is that the impedance can be imposed without having information of the line [15].

As explained in [33], the virtual impedance can consists of either a virtual resistive impedance or an inductive impedance that make the impedance more resistive or inductive respectively. Additionally due to it being virtual, the sign can easily be adjusted. This means that negative virtual inductances or resistances can be added to adjust values if needed. In some cases the virtual inductance can be implemented as [15]:

$$V^*_{new} = V^* - L_{virtual}\frac{\mathrm{di_g}}{dt} \tag{4.8}$$

Where V^* is the calculated reference voltage by the droop control. There are further variations such as using a low-pass filter instead of a derivative or having the virtual impedance change trough low bandwidth communication estimation.

Ideally the virtual impedance is added so that the line is predominantly inductive, and thus the traditional droop control can be applied efficiently. However, in the case of a low voltage micro-grid the lines are mainly resistive as shown in the previous section. Thus, if an inductance is added to compensate it will have a large value that can cause voltage drops and limit the power output of the converters [20]. Therefore, the addition of impedance in this case has to be done carefully.

The virtual impedance is implemented using the equations from [34]. These equations are shown in equations 4.9 and 4.10. The dq current components used come from the current i_g which it the output current at the grid side inductor. The obtained values are subtracted from the reference d and q voltage used in the innerloop control. Based on this, figure 4.7 can be modified to include the virtual impedance inputs. The resulting schematic is shown in figure 4.8.

$$Vv_d = i_d R_v - i_q X_v \tag{4.9}$$

$$Vv_q = i_q R_v + i_d X_v \tag{4.10}$$

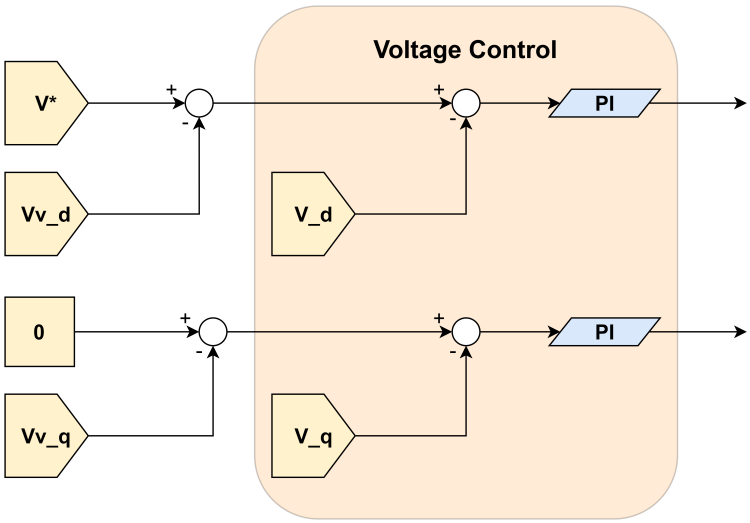

Figure 4.8: Innerloop control with virtual impedance

The virtual impedance can be seen as an offset applied to the voltage. While it helps improve how the active and reactive power is shared among the loads, it can have a negative effect on the voltage. The offset can cause the voltage of the DG to be higher or lower than under normal operation. Thus, this factor should be taken into account when deciding the values for the virtual impedance.

Although the unbalanced loads are studied in chapter 5, it is necessary to remark that if dealing with unbalanced loads a change has to be done to the virtual impedance. Instead of using i_q, one has to use the positive sequence of this current i_q^+. This avoids increasing the voltage unbalance factor (VUF) due to negative sequence voltage drop in the virtual impedance [35].

4.4 P.F/Q.V droop control simulation results

In this section the model for the DG described in the previous sections is implemented. The DGs are tested under different scenarios while using the P.F/Q.V droop control. The layout of the grid to be simulated is shown in figure 4.9. The grid consist of 3 distributed generators and 5 different possible positions for loads. The rated power for each DG is shown in table 4.2. These DGs and load E are connected by lines of different lengths. The PCC of the grid is the point where load A is connected as all the lines connecting the loads merge there. Finally, for readability in this section the active and reactive powers shown are the filtered values obtained in the droop control.

Distributed Generator	Rated Active Power (kW)
DG 1	11.7
DG 2	5.8
DG 3	23.5

Table 4.2: DG rated active power

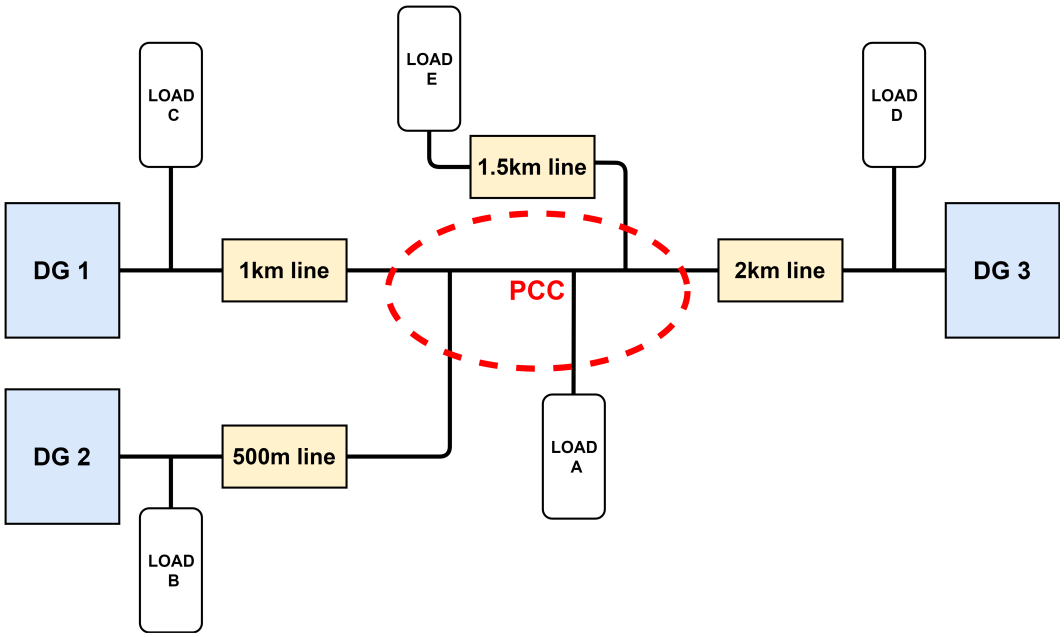

Figure 4.9: Test grid layout

4.4.1 Line distance tests

In this subsection the impact that the length of the line has on the system is demonstrated. For this demonstration the three DGs will be feeding only load A which is located at the PCC. Load A will consist of a resistive and inductive load demanding an active power of $8KW$ and a reactive power of $5k$VAR. The test done in this subsection are done without

the usage of virtual impedance in order to emphasize the influence of the line length on the system. The reference values for the droop control in each DG are set in order to share the loads accordingly to their maximum capacities. The used set-points are shown in table 4.3.

Distributed Generator	**Reference Active Power (kW)**	**Reference Reactive Power (kVAR)**
DG 1	2.5	1.5
DG 2	1.5	1
DG 3	4	2.5

Table 4.3: DG droop control set-points

For the first scenario all the lines are set to the same length of 1km. In figure 4.10 it is shown that after reaching its steady state the active power is shared indeed according to the reference power set at each DG's droop control. However, this is not the case for the reactive power. Figure 4.11 shows that the reactive power is not shared according to the set-point. DG3 which has the highest capability is the one producing the lowest amount of reactive power in this case. This low production forces the other DG to increase their output in order to compensate. One way to counter this is to set a higher reference reactive power than what is actually intended. This is how the result shown in figure 4.12 is obtained. While this is an easy solution, it affect the stability of the system and the bus voltage [36].

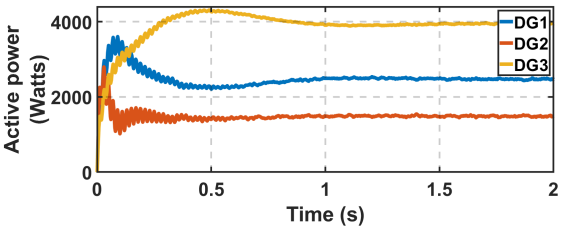

Figure 4.10: Active power generated by DGs feeding load A with lines of equal length using traditional droop control

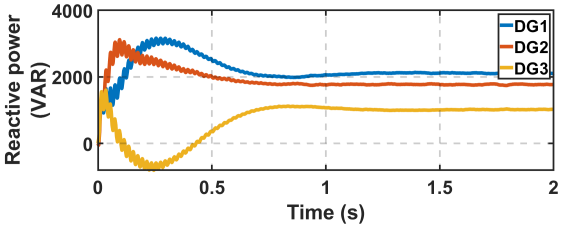

Figure 4.11: Reactive power generated by DGs feeding load A with lines of equal length using traditional droop control

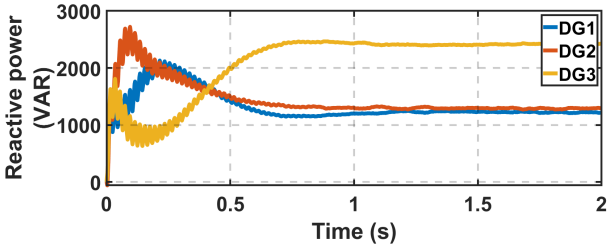

Figure 4.12: Reactive power generated by increasing DG3's set-point while feeding load A with lines of equal length using traditional droop control

Effect of a longer line

Using the previously described set-up, the length of line connecting DG 3 is increased to 2km. The obtained results are shown in figure 4.13 and figure 4.14. It can be seen that increasing the length of the line causes has an impact in the amount of reactive power that is transmitted by DG3. As a consequence the other generators have to compensate by generate more reactive power. The active power however is unaffected by this change.

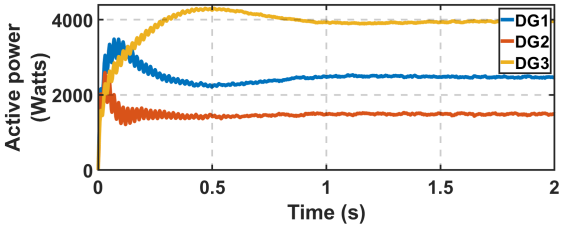

Figure 4.13: Active power generated while feeding load A with increased line length for DG3 using traditional droop control

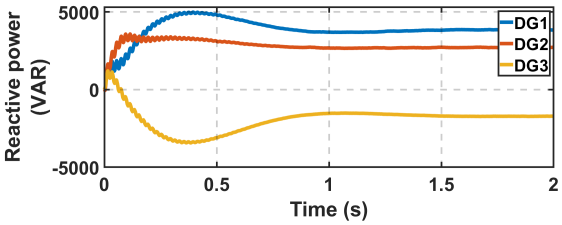

Figure 4.14: Reactive power generated while feeding load A with increased line length for DG3 using traditional droop control

Effect of a shorter line

After testing the effect of increasing a line, the opposite is done. The line connecting DG3 is returned to a length of 1km. Meanwhile, the length of the line connecting DG2 is shortened to 500m. As in the previous case, the active power remains unchanged. The reactive power generation of DG2 which has the shorter line is greater than before. This can be seen when comparing figure 4.12 to the obtained result in figure 4.16.

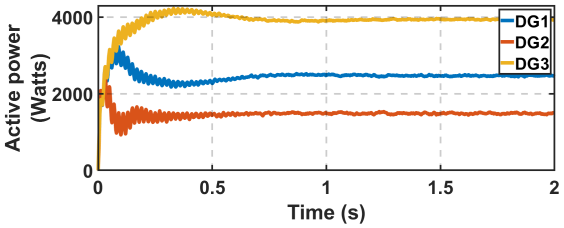

Figure 4.15: Active power generated feeding load A with shortened line length for DG2 using traditional droop control

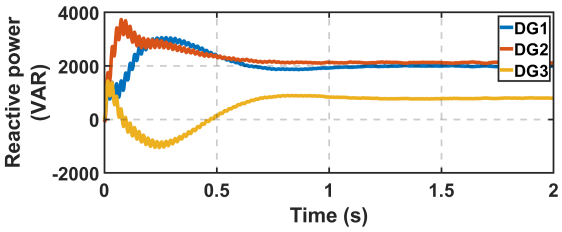

Figure 4.16: Reactive power generated feeding load A with shortened line length for DG2 using traditional droop control

Phenomena explanation

As it has been seen, the length of the line greatly affects the output powers of the DGs. This result is indeed expected. In section 3.2, it was shown that due to the mainly resistive lines the transmitted active and reactive power depends on the resistance of the line. This is detailed in equations 3.12 and 3.13. Bigger resistance leads to a smaller output, and a

smaller resistance leads to a bigger output. The value of the line resistance also affects the power angle δ which has a direct impact on the reactive power as well. This phenomena has been further studied in [20]. It was shown that two DGs with the same rated power, but different line resistances were not able to share reactive power properly. The problem of reactive power sharing can be regulated by the use of a virtual impedance. In [20], different simulation scenarios are carried out showing that the use of a virtual impedance is indeed able to ensure a better reactive power sharing.

4.4.2 Load connection tests

In this section the ability of the micro-grid to stand the connection of new loads is evaluated. This includes connection of a resistive and inductive load, a purely resistive loads, a purely inductive loads, and a purely capacitive load. Table 4.4 shows different information about the loads such as their position in the grid, their time of connection, and different values. In table 4.4 the inductive loads are represented by a positive reactive power. Meanwhile, capacitive loads are represented by a negative reactive power. The lines connecting the DGs have the different lengths specified in figure 4.9

Load	**Time of connection (s)**	**Active Power (kW)**	**Reactive Power (kVAR)**
A	0	8	5
B	2	4	1
C	4	0	3
D	6	0	-3
E	8	5	0

Table 4.4: Load connection time and values

Connection at PCC

First, adding multiple loads to the point of common coupling is evaluated. For this test loads A trough E are connected at the PCC. This means connecting multiple loads at the connection point of load A in figure 4.9. The time of connection will follow the one specified in table 4.4

No virtual impedance In the previous section it was already shown that having lines of different length has an impact on the system in terms of reactive power sharing. The response of the micro-grid to multiple connections at the PCC is shown here to further emphasize this point.

Figure 4.17 shows that the active power is shared according to the set-point and the capacity of each DG. This is possible due to the fact that the frequency has the same value across the grid. The response for the reactive power is shown in figure 4.18. The micro-grid is indeed responding to the changes in demand for reactive power. However, DG3 produces negative reactive power while DG1 and DG2 produce positive. This contradiction leads to unnecessary high values of reactive power.

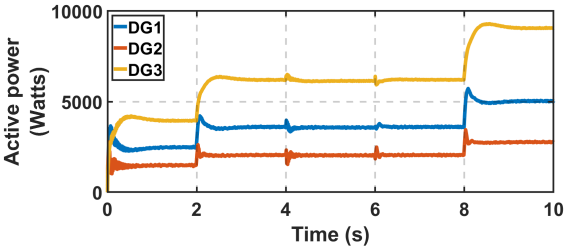

Figure 4.17: Active power generated by DGs with no virtual impedance and with loads connecting only to PCC using traditional droop control

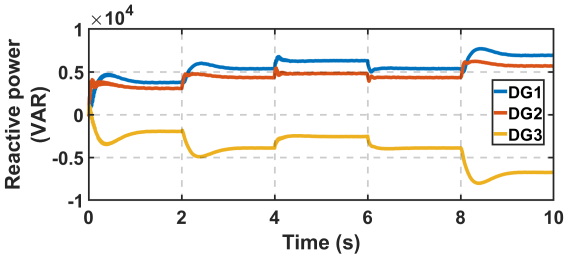

Figure 4.18: Reactive power generated by DGs with no virtual impedance and with loads connecting only to PCC using traditional droop control

In the two previous pictures and in the following results, it can be appreciated that the signals have an oscillation or ripple to them. Indeed, even after the transient the signal settles around a value, but it does not remain steady. This is due to the way the droop control and the inner loop work. Small variations in the power generated will correspond to small variations to the voltage and frequency. These variations will be enter the PI controllers of the innerloop as well. In addition, all of the DGs are oscillating which to a lesser extent also influences the other DGs. Thus, the values found during the different tests are no steady, but instead oscillate around a value.

The undesired response of the reactive power has an effect in the voltage due to the droop control. Ideally, generating reactive power under the set-point would lead to a higher reference voltage. In exchange, being above the set-point would lead to a lower reference voltage. Figure 4.19 shows the Root Mean Square (RMS) voltage of phase A in each DG. DG1 and DG2 show the expected behaviour. However, it is shown that the voltage of DG3 is rising contrary to the other DGs. This is because the reactive power being produced is negative and thus results to an increase in the reference voltage generated by the droop control. Figure 4.20 demonstrates how the currents change with the connection of the loads. Due to the production of reactive power the currents of DG3 and DG2 are close to the same value.

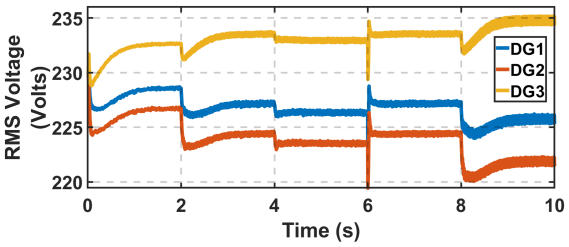

Figure 4.19: RMS voltage of DGs with no virtual impedance and with loads connecting only to PCC using traditional droop control

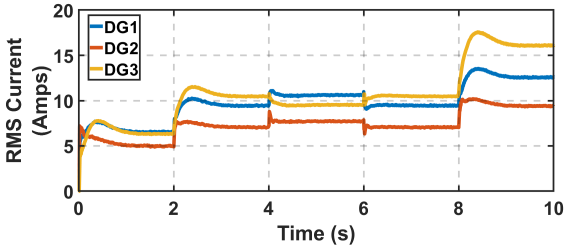

Figure 4.20: RMS current of DGs with no virtual impedance and with loads connecting only to PCC using traditional droop control

As mentioned before, the micro-grid frequency is has the same value for all the DGs unlike the voltage. Thus the active power is properly shared among the DGs. This is why the drop in frequency at $t = 2s$ and $t = 8s$, which is linked to the increase in active power, causes and equal drop in the reference value among the different DGs. This same fact can be attributed for the spikes in frequency when a load is connected. Any spike in active power will be reflected in the frequency due to the droop control mechanism. The bigger spikes in frequency occur at t=4s and t=6s which correspond to the connection of purely inductive and purely capacitive loads respectively.

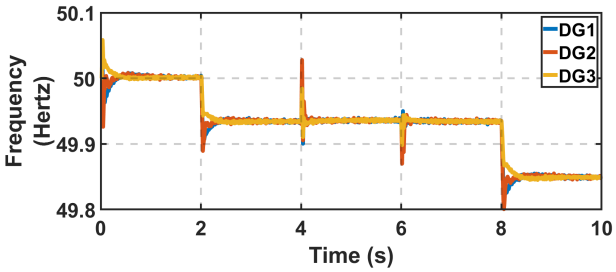

Figure 4.21: Frequency of DGs with no virtual impedance and with loads connecting only to PCC using traditional droop control

With virtual impedance The same experiment is repeated except the DGs are now using virtual impedances in their control loop. The active power is shared according to the capacity of each DG as it is shown in figure 4.22. It is worth noticing that adding the virtual impedance dampens the response and thus creates lower peaks at the connection of each load and the startup. Figure 4.23 shows that the reactive power generation is indeed improved through the use of virtual impedance. DG3 is able to produce positive reactive power and better contribute towards sharing the loads.

It can be seen that the reactive power of DG3 decreases unexpectedly at $t = 2s$ and $t = 8s$. At $t = 2s$ a increase in active and reactive power is supposed to take place, and at $t = 8s$ no change should happen in the reactive power. This can be explained by the fact that traditional droop control is being applied on mainly resistive lines. As explained in section 3.2 and section 3.3 mainly resistive lines lead to a different set of equations which

are equations 3.12 and 3.13. Applying traditional P.F/Q.V droop control on such lines leads to coupling between the two droop controls. The drops in reactive power are then related to the increase in active power demanded at those times.

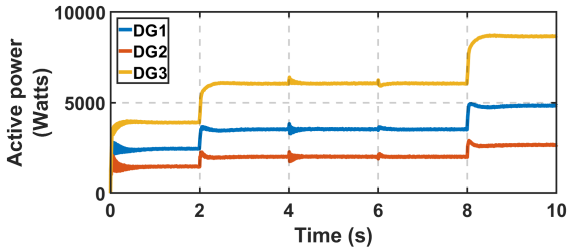

Figure 4.22: Active power generated by DGs with virtual impedance and with loads connecting only to PCC using traditional droop control

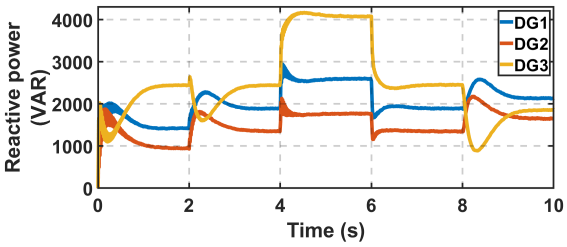

Figure 4.23: Reactive power generated by DGs with virtual impedance and with loads connecting only to PCC using traditional droop control

In figures 4.24 and 4.25 the RMS value for one phase of the voltage and current are shown. Although the reactive power response is better than without the virtual impedance, figure 4.24 shows a similar voltage response to the case without the virtual impedance. This is due to the addition of the virtual impedance. DG1 and DG2 have a positive virtual impedance that result in a further reduction of the reference voltage. Meanwhile, DG3 has a negative ritual impedance that makes its final voltage value increase. Thus, the voltage response will depend on changes cause by the droop control and the interactions of the output current with the virtual impedance. For example at $t = 4s$, the RMS voltage of DG3 lowers itself instead of increasing. This is because the decrease in the reference voltage generated by the droop control is bigger than the increase caused by the current interacting with the virtual impedance. Figure 4.25 shows that thanks to the virtual impedance the currents are lower for DG1 and DG2. This is because the loads are better distributed among the DGs. However, as discussed previously the voltage suffers due to the addition of the virtual impedance.

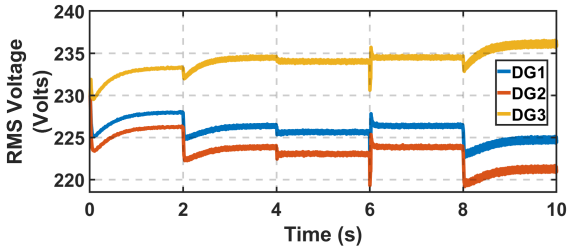

Figure 4.24: RMS voltage of DGs with virtual impedance and with loads connecting only to PCC using traditional droop control

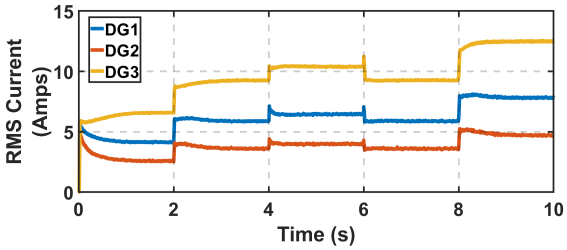

Figure 4.25: RMS current of DGs with virtual impedance and with loads connecting only to PCC using traditional droop control

Finally, in figure 4.26 shows the frequency at each DG. Since the active power was correctly managed in both cases, the frequency response shown is similar and acts according to the expectations. Once again the bigger spikes occur during the connection of purely inductive and purely capacitive loads.

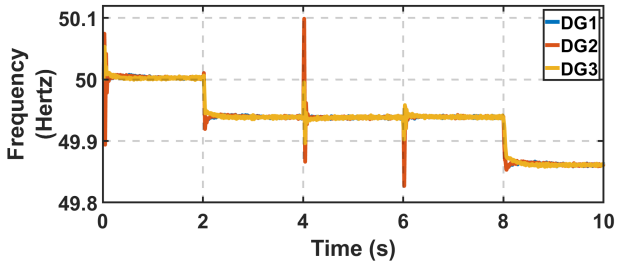

Figure 4.26: Frequency of DGs with virtual impedance and with loads connecting only to PCC using traditional droop control

Dispersed loads connection

For this test the loads are distributed across the grid. They are placed in the positions described in figure 4.9. The connection times and values are the ones shown in table 4.4. Because of the improvements shown before, this and the following tests are done while using a virtual impedance on each DG.

As in the case of loads at the PCC, the active power follows the set-points, and it is shared among the DGs according to their capacity. This result is shown in figure 4.27. The reactive power behaves differently than when all the loads are connected at the PCC. In figure 4.28, it is shown that the distance of the load with respect to the DG has an effect on the reactive power generated. This can be first seen at $t = 2s$ when load B is connected. Load B is connected next to DG2 which assumes almost all the production of the reactive power requested by the load. Another point where such a behaviour can be seen is at $t = 6s$ that corresponds to the connection of load D. It is seen that DG3 takes most of the generation of the capacitive power requested. As a consequence, it is the DG that drops its reactive power generation the most.

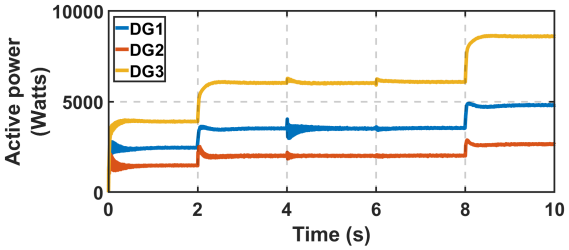

Figure 4.27: Active power generated by DGs with virtual impedance and with loads connecting to different points on the grid using traditional droop control

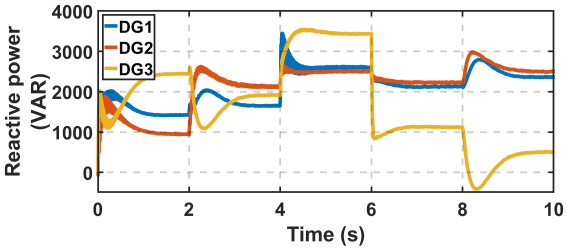

Figure 4.28: Reactive power generated by DGs with virtual impedance and with loads connecting to different points on the grid using traditional droop control

The RMS voltage shown in figure 4.29 follows the behaviour caused by the interaction of the droop control and the virtual impedance as explained in the previous test. Equally, the current in figure 4.30 is changing accordingly to the connection of the loads. Additionally, it shows that their contribution is in accordance to their rated capacity.

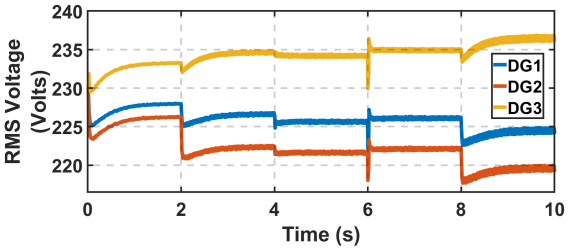

Figure 4.29: RMS voltage of DGs with virtual impedance and with loads connecting to different points on the grid using traditional droop control

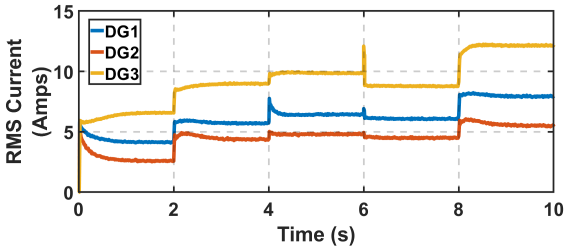

Figure 4.30: RMS current of DGs with virtual impedance and with loads connecting to different points on the grid using traditional droop control

As in the previous test, the frequency shown in figure 4.31 is very accurately regulated as it is directly linked to the active power. Again, at $t = 8s$ load E which purely resisitive causes a demand in active power. This causes a small decrease in the frequency of each DG. The connection of the purely inductive load C at t=4s causes a spike in the frequency. In this case load C is next to DG1, it can be seen that the DG that suffers the biggest spike in frequency is indeed DG1.

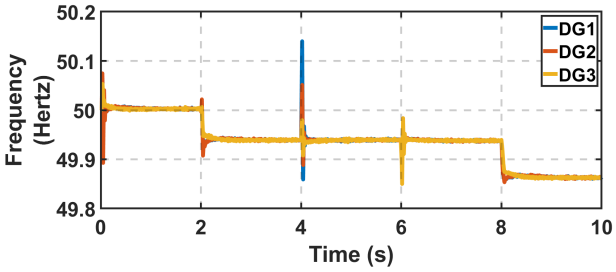

Figure 4.31: Frequency of DGs with virtual impedance and with loads connecting to different points on the grid using traditional droop control

4.4.3 Load and DG disconnection

To further test the reliability of the system two more tests are done. One of them is connecting the loads and then disconnecting them to test the reaction of the micro-grid. The second test is the compensation system of the micro-grid when a DG is disconnected.

Load disconnection

Loads A through C are connected as stated on table 4.4. Load C is disconnected two seconds after its connection. After two more seconds load B is disconnected. As it can be seen from figures 4.32 to 4.36, the system is able to return to its previous steady state after experiencing a transient caused by each disconnection. The disconnection of each load as its connection affect mostly the DG close to its connection point.

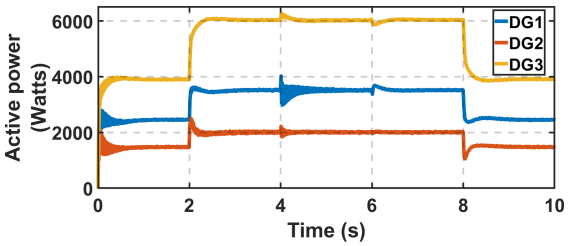

Figure 4.32: Active power generated by DGs with virtual impedance and with loads disconnections using traditional droop control

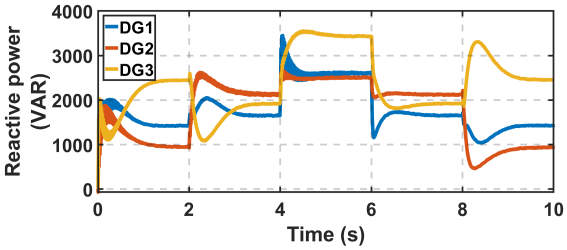

Figure 4.33: Reactive power generated by DGs with virtual impedance and with loads disconnections using traditional droop control

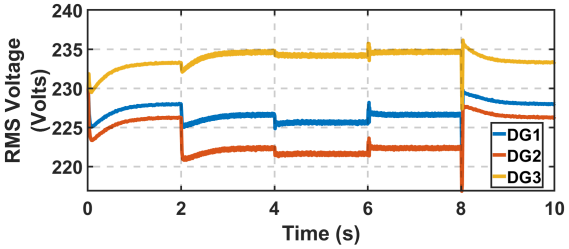

Figure 4.34: RMS voltage of DGs with with virtual impedance and with loads disconnections using traditional droop control

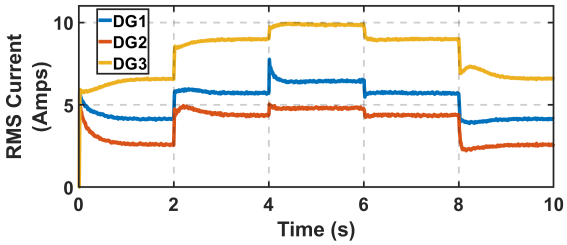

Figure 4.35: RMS current of DGs with virtual impedance and with loads disconnections using traditional droop control

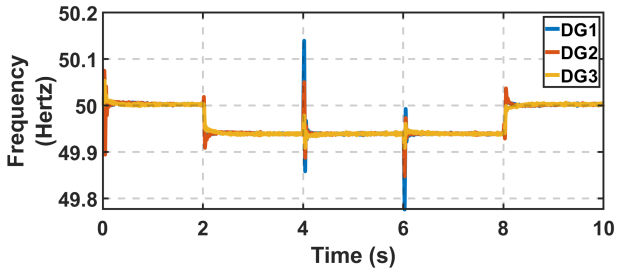

Figure 4.36: Frequency of DGs with virtual impedance and with loads disconnections using traditional droop control

DG disconnection

The ability of the micro-grid to handle the disconnection of a distributed generator is shown in the following figures. For this test, loads A through C are connected following the time and values of table 4.4. At time $t = 6$ DG3 is disconnected from the micro-grid. In figures 4.37 and 4.38 it is shown that the other two generators increase their production of both active and reactive power in order to compensate the disconnection of DG3. DG1 has to increase its production more as DG2 reaches its active power production limit.

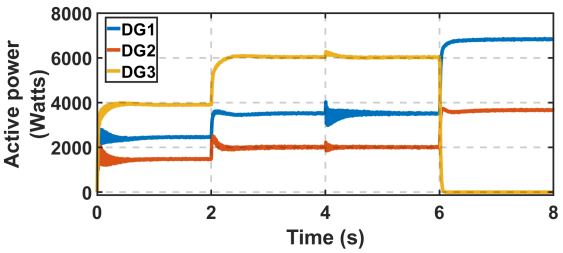

Figure 4.37: Active power generated by DGs with virtual impedance and with disconnection of DG3 using traditional droop control

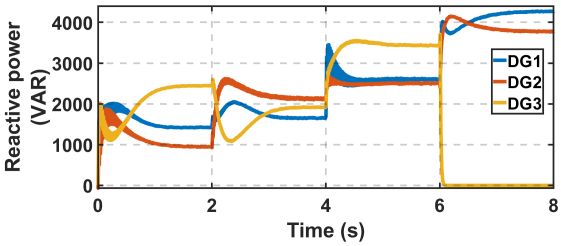

Figure 4.38: Reactive power generated by DGs with virtual impedance and with disconnection of DG3 using traditional droop control

The voltage as shown in figure 4.39 demonstrates that the compensation by the two DGs cause its RMS voltage to drop. As DG3 is not producing any type of power its RMS voltage decreases. It is not exactly at 230V due to the behaviour of the droop control. This happens because the reference reactive power is subtracted to the current reactive power output which is zero. The resulting negative value is then multiplied by the droop coefficient and subtracted from the reference value. Thus resulting in a new reference value higher than 230V.

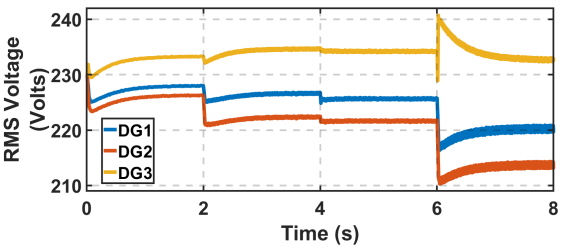

Figure 4.39: RMS voltage of DGs with virtual impedance and with disconnection of DG3 using traditional droop control

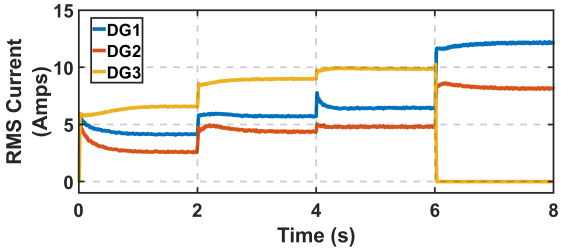

Figure 4.40: RMS current of DGs with virtual impedance and with disconnection of DG3 using traditional droop control

In Figure 4.41 the frequency of DG1 and DG2 drops as the power generation increased. The frequency of DG3 increases as it behaves similarly to the voltage. In this case, the reference active power value is compared to the current active power output thus causing a rise in the reference value as explained previously.

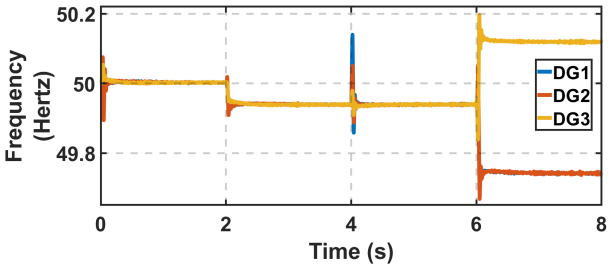

Figure 4.41: Frequency of DGs with virtual impedance and with disconnection of DG3 using traditional droop control

4.4.4 Starting of an asynchronous motor

Finally, the starting of an asynchronous motor is used as a final test. This motor has a capacity of 4kW. It will be connected at the PCC along with load A. First, the grid is started with only load A connected. Once the grid has stabilized the motor is connected at time $t = 3s$ with a torque of zero. After the transient due to the sudden connection is gone, the torque is increased from zero to one. A ramp in the torque starts at $t = 3.3s$ until it reaches its nominal value.

The obtained results through figures 4.42 to 4.46 show that the connection of the motor causes a strong transient on the grid. This transient leads to an increase in active and reactive power, but quickly returns to the previous values. The ramp of the torque is clearly seen in the active power shown in figure 4.42. In figure 4.43 a change in the reactive power can also be appreciated as well. The voltage, current, and frequency change as the torque is increased as shown in figures 4.44, 4.45, and 4.46.

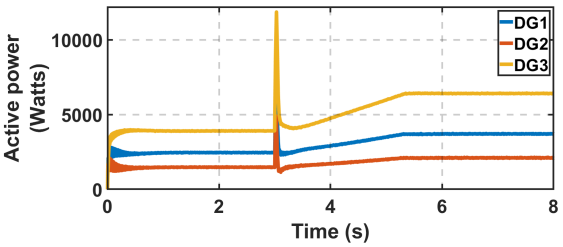

Figure 4.42: Active power generated by DGs with virtual impedance and with a motor load using traditional droop control

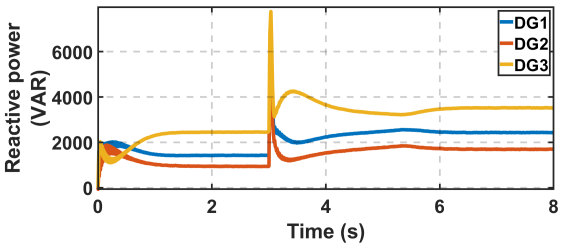

Figure 4.43: Reactive power generated by DGs with virtual impedance and with a motor load using traditional droop control

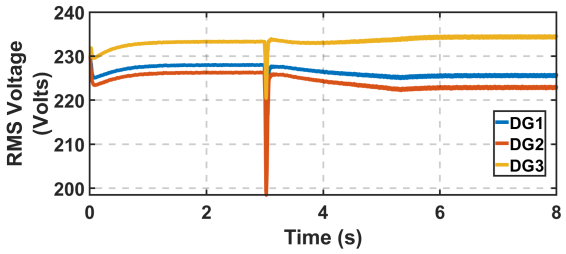

Figure 4.44: RMS voltage of DGs with virtual impedance and with a motor load using traditional droop control

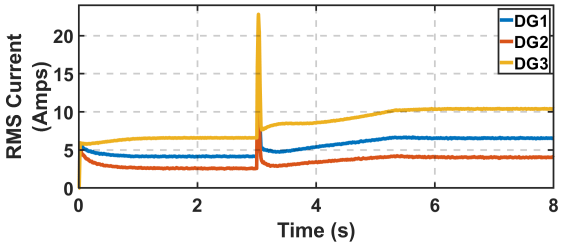

Figure 4.45: RMS current of DGs with virtual impedance and with a motor load using traditional droop control

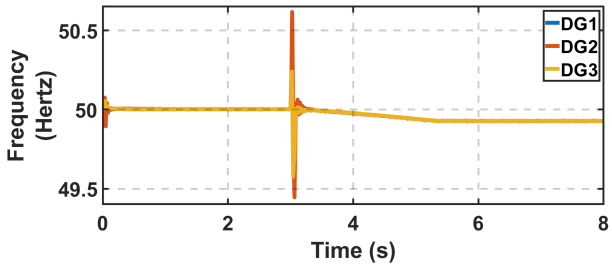

Figure 4.46: Frequency of DGs with virtual impedance and with a motor load using traditional droop control

The previous results indicate that the system is reacting as expected to the connection of the motor. To further confirm this, two values of the motor are also analyzed. Figure 4.47 shows the electromagnetic torque of the motor. This value is increases until it reaches a value of 1. As it is in a per unit system this would be equivalent to the full load of 4kW. Figure 4.48 shows the evolution of the rotor speed. It is kept close to 1, and after the ramp has finished it remains at the same value. This indicates that the motor is operating properly, and thus the micro-grid is indeed able to handle the connection of an asynchronous motor.

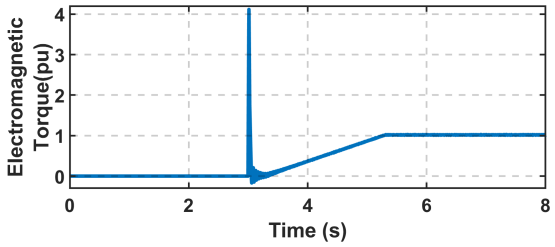

Figure 4.47: Motor electromagnetic torque with virtual impedance and using traditional droop control

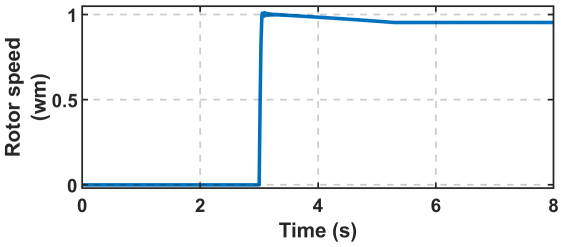

Figure 4.48: Motor rotor speed with virtual impedance and using traditional droop control

4.5 P.V/Q.F droop control simulation results

In this section the P.V/Q.F droop control is tested under the same scenarios as the P.F/Q.V droop control. Thus, the same grid structure shown in figure 4.9 is used. Equally, the loads described have the same values and connecting times as it was shown in table 4.4. Finally, the set-points for power and reactive power generation remain as stated in table 4.3.

4.5.1 Line distance tests

The effect of changing the line length on this type of droop control is tested. First, it is considered that only load A is connected, and that all the lines have the same length of 1km. Figure 4.49 shows that DG3 is producing the most active power as it should. However, the distribution of the load among the DGs is not done equally. Further more, the DGs are not at their requested set-points. Meanwhile, the reactive power shown in figure 4.50 is indeed shared according to the requested set-points. This shows that in the P.V/Q.F droop control the reactive power is controlled precisely while the active power has some inaccuracies. The opposite was true for the P.F/Q.V droop control as it has been explored in the previous section. The P.F/Q.V droop control has precise control over the active power and inaccuracies in the reactive power. A comparison can be made by looking at figures 4.49 and 4.50 of the opposite droop control against the figures 4.10 and 4.11 of the traditional droop control. When both control methods are compared without virtual impedance it can be seen that the traditional droop's inaccuracies are more significant. Additionally the time taken to reach the steady value after the initial transient is longer for the traditional droop. While the P.V/Q.F droop has some inaccuracies in the power control, it presents a better transient behaviour and overall accuracy than the P.F/Q.V droop control.

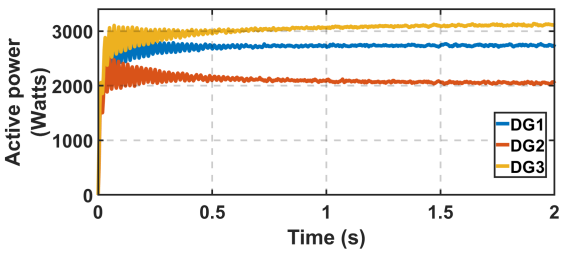

Figure 4.49: Active power generated by DGs feeding load A with lines of equal length using opposite droop control

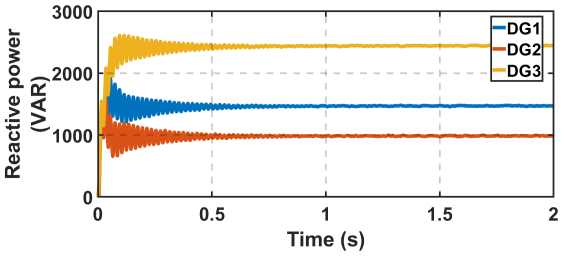

Figure 4.50: Reactive power generated by DGs feeding load A with lines of equal length using opposite droop control

Effect of a longer line

Using the previously described set-up, the length of the line connecting DG 3 is increased to 2km. The active power in figure 4.51 shows that the power of DG3 decreases as the line length increases. This behaviour mirrors that of the reactive power in the P.F/Q.V droop control under the same circumstances in figure 4.16. The reactive power in figure 4.52 remains unaffected.

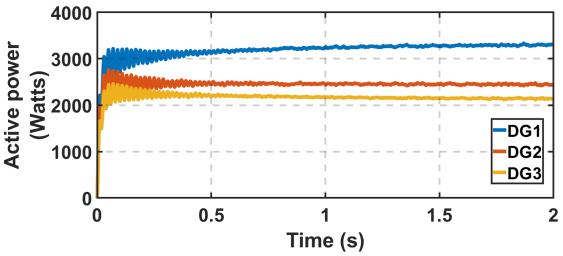

Figure 4.51: Active power generated while feeding load A with increased line length for DG3 using opposite droop control

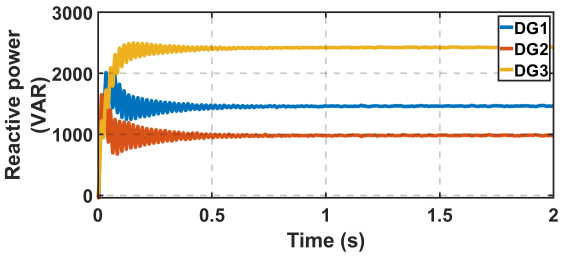

Figure 4.52: Reactive power generated while feeding load A with increased line length for DG3 using opposite droop control

Effect of a shorter line

The line connecting DG3 is returned to a length of 1km. Meanwhile, the length of the line connecting DG2 is shortened to 500m. The active power generation of DG2 increases as shown in figure 4.53. As in the previous cases the reactive power in figure 4.54 remains mainly unchanged.

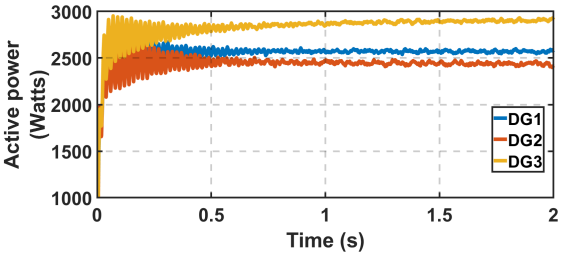

Figure 4.53: Active power generated feeding load A with shortened line length for DG2 using opposite droop control

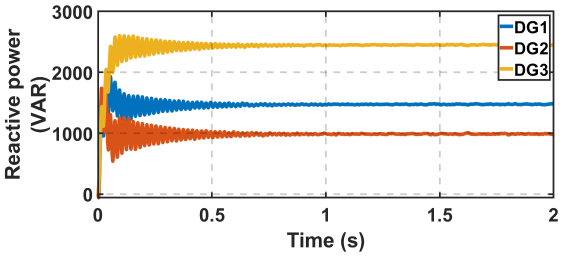

Figure 4.54: Reactive power generated feeding load A with shortened line length for DG2 using opposite droop control

4.5.2 Load connection tests

In this section the capability of the P.V/Q.F droop control to manage the connection of multiple loads is evaluated. As stated before, the loads correspond to the values and connection times described in table 4.4 as in the previous section.

Connection at PCC

First, loads A through E will be connected at the PCC. This will be first done with the innerloop control unmodified. The test will be then repeated, but adding a virtual impedance to the inner loop control to see if it is able to improve its performance.

No virtual Impedance Figures 4.55 and 4.56 show how the active and reactive power is evolving as the loads are connected. The active power is adjusted properly to the loads, but it is not distributed among the loads according to their rated power. The reactive power is adjusted without any problems. Overall, the P.V/Q.F droop control manages the power better than the P.F/Q.V droop control under the same scenario.

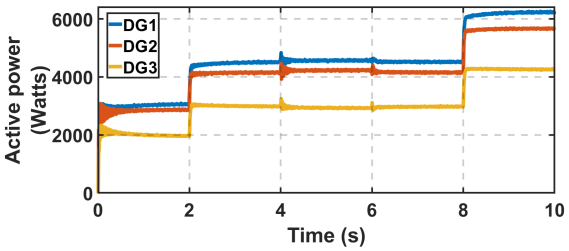

Figure 4.55: Active power generated by DGs with no virtual impedance and with loads connecting only to PCC using opposite droop control

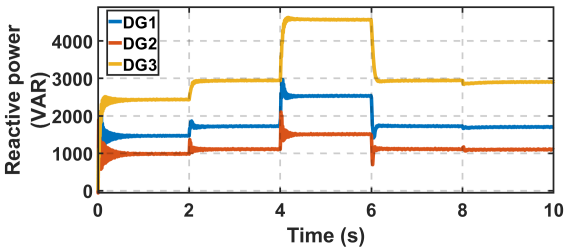

Figure 4.56: Reactive power generated by DGs with no virtual impedance and with loads connecting only to PCC using opposite droop control

The voltage of the DGs is indeed decreased as the active power is increased as shown in figure 4.57. However, DG3 has a voltage above the expected 230V as it is providing less power than what is specified by the set-point of the droop control. The active power is not provided according to the rated power of each DGs. This causes the current generated by each DG to be close to each other. This can be seen in figure 4.58.

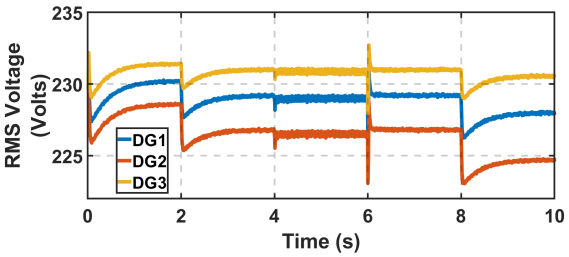

Figure 4.57: RMS voltage of DGs with no virtual impedance and with loads connecting only to PCC using opposite droop control

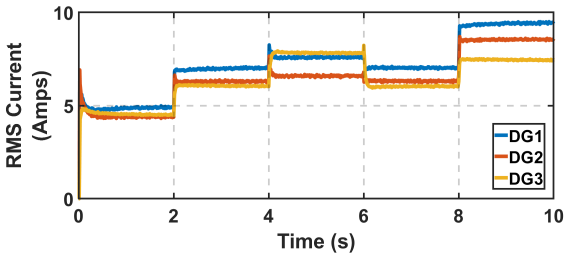

Figure 4.58: RMS current of DGs with no virtual impedance and with loads connecting only to PCC using opposite droop control

In the P.V/Q.F droop control the frequency is linked to the reactive power. Thus the changes in frequency seen in figure 4.59 are closely linked to the changes in reactive power generation due to the addition of the loads. This implies that spikes in reactive power production will also be reflected in the frequency. Once again two major spikes can be seen at t=4s and t=6s. These correspond to the connection of a purely inductive load at t=4s and a purely capacitive load at t=6s.

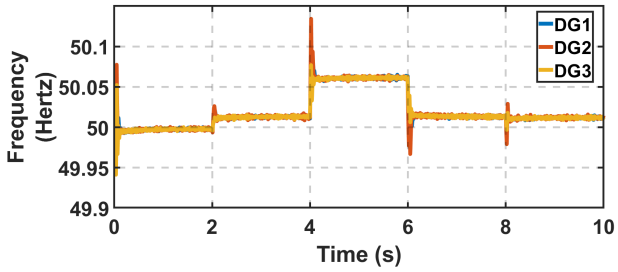

Figure 4.59: Frequency of DGs with no virtual impedance and with loads connecting only to PCC using opposite droop control

With virtual Impedance In order to correct the inaccuracies previously shown, a virtual impedance is added to the innerloop control of each DG. Figure 4.60 shows the impact the virtual impedance has on the load distribution. The power is now shared accordingly to the rated power of each DG. As seen DG3 is now the one providing the majority of the active power. The reactive power as in the original scenario is shared as desired. Once again, the reaction of the P.V/Q.F droop control to the connection of loads is significantly better than the P.F./Q.V under the same conditions.

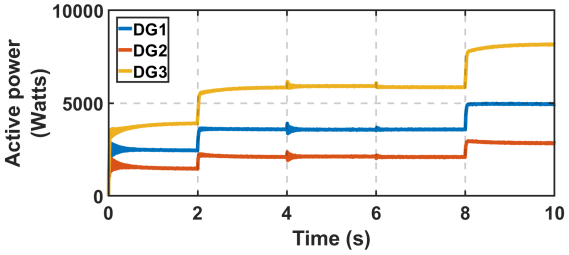

Figure 4.60: Active power generated by DGs with virtual impedance and with loads connecting only to PCC using opposite droop control

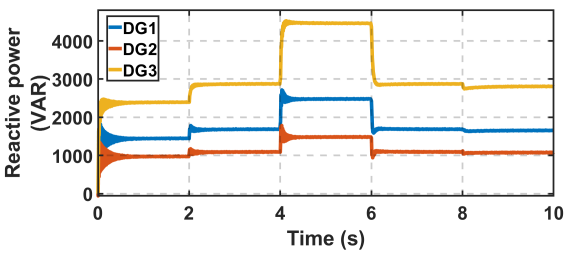

Figure 4.61: Reactive power generated by DGs with virtual impedance and with loads connecting only to PCC using opposite droop control

The behaviour of the voltage is affected by the inclusion of the virtual impedance. As in the case of the P.F/Q.V droop control, the virtual impedance for DG1 and DG2 is positive. Meanwhile, the virtual impedance for DG3 is negative. The negative virtual impedance causes DG3 to increase its output voltage proportionally to the current. The voltage can still decrease if the voltage drop specified by the droop control is higher than the increase caused by the current. While the voltage is sightly degraded, the currents

shown in figure 4.63 are better distributed according to the capacity of their respective DG.

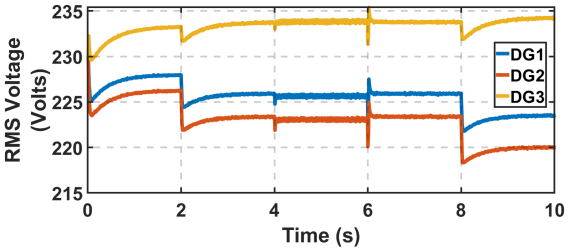

Figure 4.62: RMS voltage of DGs with virtual impedance and with loads connecting only to PCC using opposite droop control

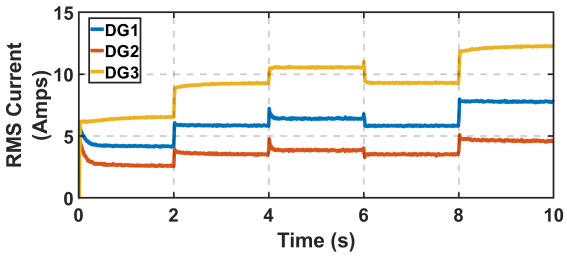

Figure 4.63: RMS current of DGs with virtual impedance and with loads connecting only to PCC using opposite droop control

As shown in figure 4.64 the frequency response remains mostly unaffected by the addition of the virtual impedance. This is convenient as it was already responding accordingly to the changes in the reactive power production.

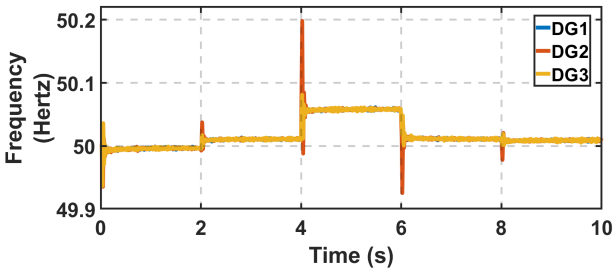

Figure 4.64: Frequency of DGs with virtual impedance and with loads connecting only to PCC using opposite droop control

Dispersed loads connection

To further test the reliability of this type of droop control, the same loads are connected with the timing of table 4.4, but now at their respective position across the grid shown in figure 4.9. Because of the improvement shown, this and the tests to follow are done using a virtual impedance on each DG.

The response of the active and reactive power is only sightly affected by this change. The DGs react sightly more to the loads closer to them. In the active power of figure 4.65 it is shown that DG2 increases its power output at $t = 2s$ more than when the loads where at the PCC. This is due to the fact that load B which has a resistive component is closer to DG2. This is shown also in the reactive power at $t = 4s$ when load C which is inductive is connected. DG1 which is next to load C shows a higher transient caused by the connection when compared to the other DGs or itself in the connection at PCC scenario. Equally, at $t = 6s$ DG3 shows a bigger dip in reactive power due to the connection of the capacitive load.

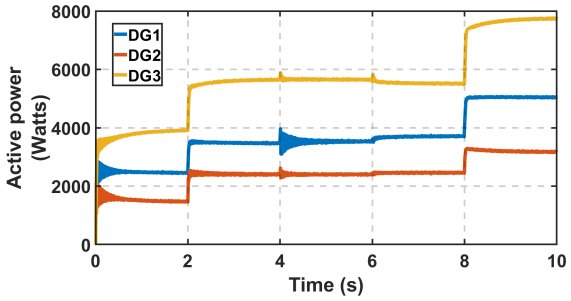

Figure 4.65: Active power generated by DGs with virtual impedance and with loads connecting to different points on the grid using opposite droop control

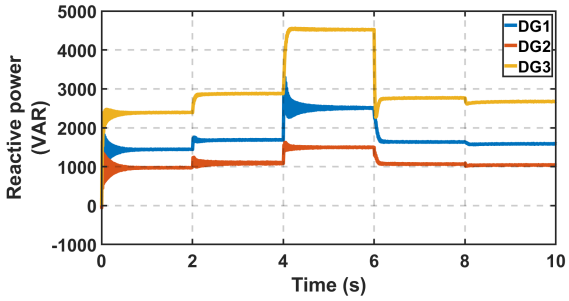

Figure 4.66: Reactive power generated by DGs with virtual impedance and with loads connecting to different points on the grid using opposite droop control

The changes in active and reactive power production are also reflected in the current and voltage. In figure 4.67 the voltage of DG1 dips deeper due to its increased active power production. If the current of DG1 in figure 4.68 is compared to the one of DG1 in figure 4.63, one can observe a more pronounced spike at $t = 4s$. The same can be seen for the dip in current of DG3 at $t = 6s$.

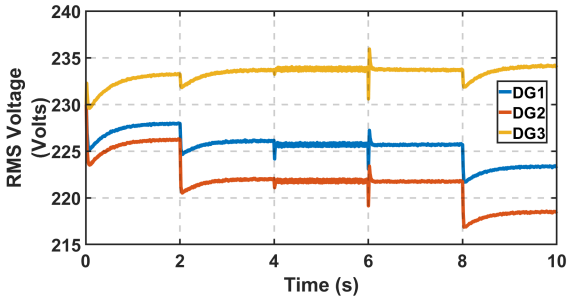

Figure 4.67: RMS voltage of DGs with virtual impedance and with loads connecting to different points on the grid using opposite droop control

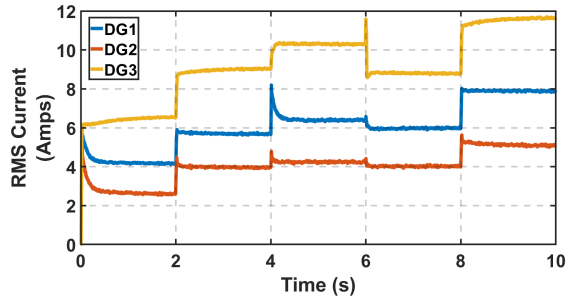

Figure 4.68: RMS current of DGs with virtual impedance and with loads connecting to different points on the grid using opposite droop control

The frequency response is kept as in the previous scenarios. Again, the two bigger frequency spikes occur when the purely inductive load C and the purely capacitive load D are connected. The main difference is that DG1 presents a bigger spike in the frequency at $t = 4s$. This is due to the mainly inductive load C being connected next to DG1.

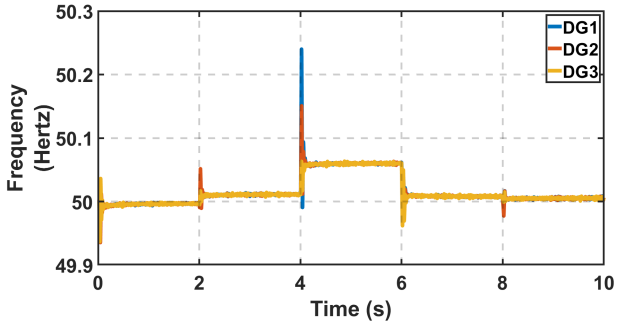

Figure 4.69: Frequency of DGs with virtual impedance and with loads connecting to different points on the grid using opposite droop control

4.5.3 Load and DG disconnection

The same tests done with the P.F/Q.V droop control are repeated here with the P.V/Q.F droop control. These tests are the disconnection of loads, and the disconnection of a DG.

Load disconnection

Loads A through C are connected leaving a 2 seconds interval between each connection. Two seconds after the connection of load C, load C is disconnected from the grid. Two seconds after load C is disconnected load B is disconnected as well. Since the loads are spread across the grid their connections and disconnections affect sightly more the DGs immediately next to them. Figures 4.70 through 4.74 show that the system with the P.V/Q.F droop control remains stable through these changes.

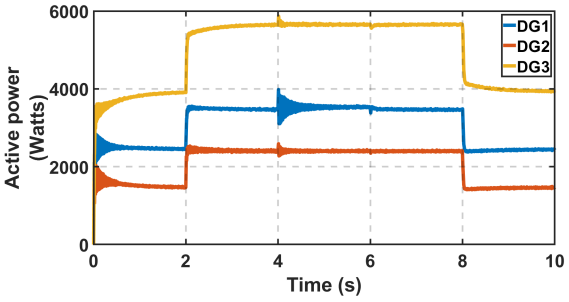

Figure 4.70: Active power generated by DGs with virtual impedance and with loads disconnections using opposite droop control

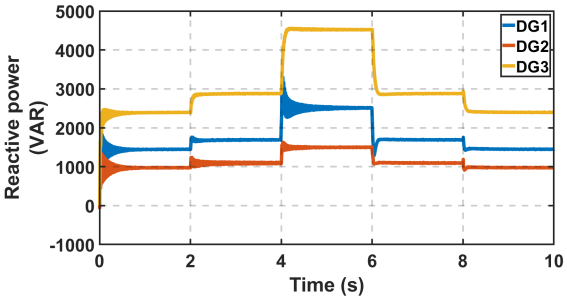

Figure 4.71: Reactive power generated by DGs with virtual impedance and with loads disconnections using opposite droop control

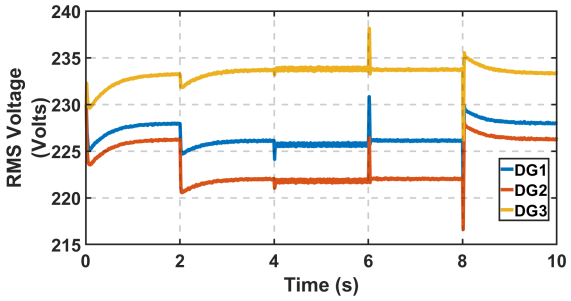

Figure 4.72: RMS voltage of DGs with virtual impedance and with loads disconnections using opposite droop control

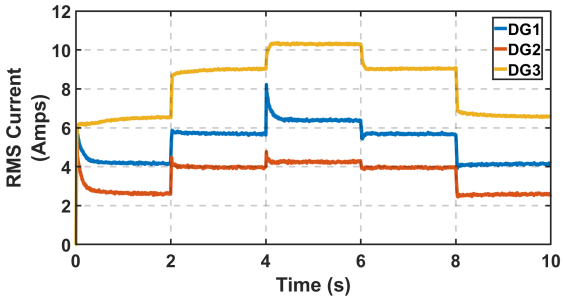

Figure 4.73: RMS current of DGs with virtual impedance and with loads disconnections using opposite droop control

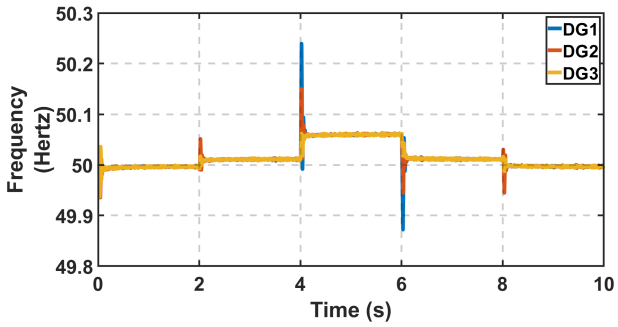

Figure 4.74: Frequency of DGs with virtual impedance and with loads disconnections using opposite droop control

DG disconnection

The capability of the system to recover from the disconnection of one DG is analyzed. For this test, loads A through C are connected to the grid at their respective times, and at $t = 6s$ DG3 is disconnected from the grid. Due to its disconnection, DG3 stops contributing active and reactive power. Thus, DG1 and DG2 need to increase their output in order to compensate. This increase in output is done effectively as shown in both figure 4.75 and figure 4.76.

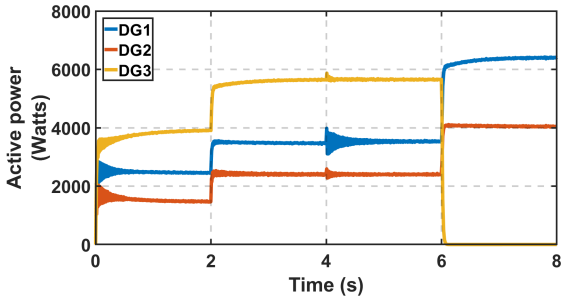

Figure 4.75: Active power generated by DGs with virtual impedance and with disconnection of DG3 using opposite droop control

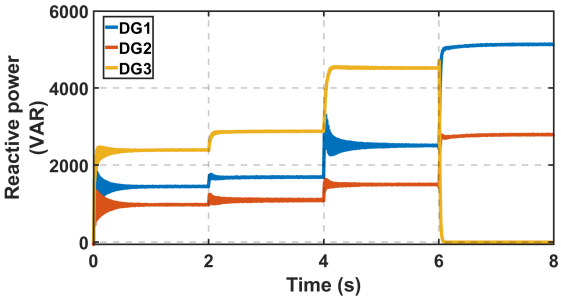

Figure 4.76: Reactive power generated by DGs with virtual impedance and with disconnection of DG3 using opposite droop control

The voltage of DG3 does not return to the rated value of 230V as the set-point of the P.V droop increases the reference voltage when the input power is equal to zero. Meanwhile, DG1 and DG2 increase their power output thus causing a drop in the voltage as seen figure 4.77. Because of the disconnection of DG3, the current of DG3 drops to zero and the currents of DG1 and DG2 increase as shown in figure 4.78.

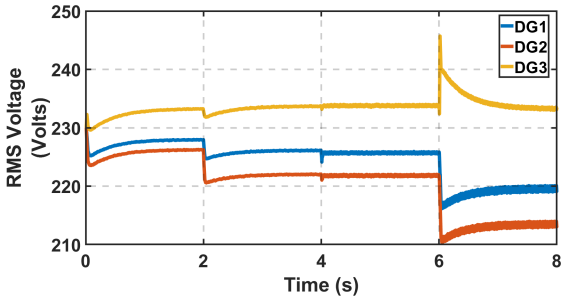

Figure 4.77: RMS voltage of DGs with virtual impedance and with disconnection of DG3 using opposite droop control

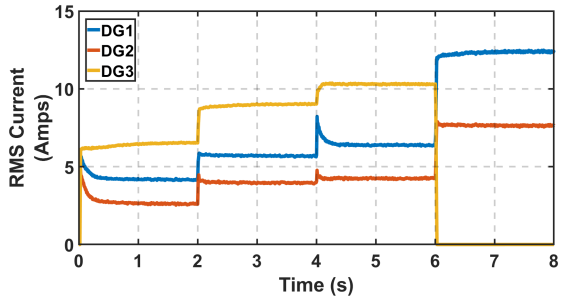

Figure 4.78: RMS current of DGs with virtual impedance and with disconnection of DG3 using opposite droop control

In terms of frequency, DG3 does not return to 50Hz because of the droop offset. Since the Q.F droop used has a positive slope, a value below the set-point will cause a decrease. On the other hand, a value above the set-point will cause the frequency to increase. This is why the frequency of DG3 goes to a value below 50Hz as it is illustrated in figure 4.79

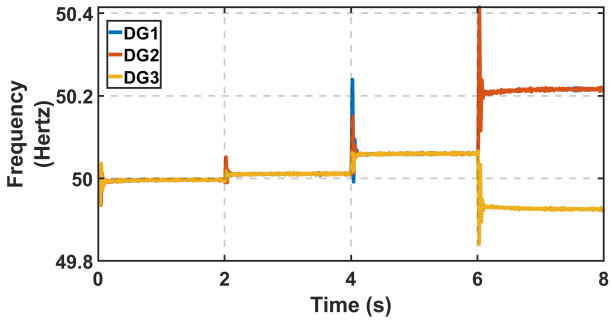

Figure 4.79: Frequency of DGs with virtual impedance and with disconnection of DG3 using opposite droop control

4.5.4 Starting of an asynchronous motor

As in the P.F/Q.V droop control, the last test done is the starting of an asynchronous machine on the grid. The same test procedure is repeated which is connecting the machine at $t = 3s$ with a torque of zero. At $t = 3.3s$ after the system recovers from the connection transient, the torque is increased until the machine reaches its nominal value. The results shown below demonstrate that the P.V/Q.F droop control does not inhibit the capability of the grid of starting such a machine.

The results obtained for both types of control are similar, but the P.V/Q.F droop control show some improvements. In terms of active power the response is mostly the same as illustrated in figure 4.80. The response of the reactive power is different however. The peak due to the connection of the motor is higher as seen in figure 4.81, but each DG stabilizes their reactive power output quickly after this transient. A big contrast can be seen when compared with its P.F/Q.V counter part seen in figure 4.43. The dip in the voltage in figure 4.82 is smaller. Because the reactive power is more stable, the evolution of the current is more stable as well. This result can be observed in figure 4.83. Finally, the frequency has a bigger peak and a different shape for the transient as it is linked with the reactive power.

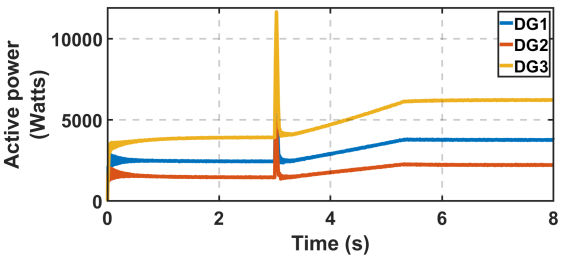

Figure 4.80: Active power generated by DGs with virtual impedance and with a motor load using opposite droop control

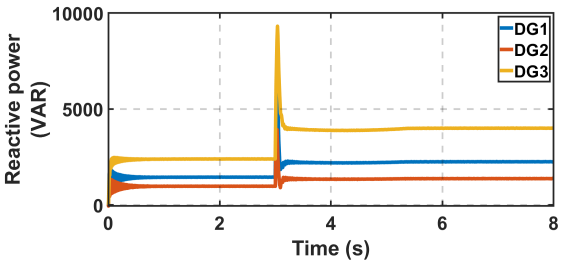

Figure 4.81: Reactive power generated by DGs with virtual impedance and with a motor load using opposite droop control

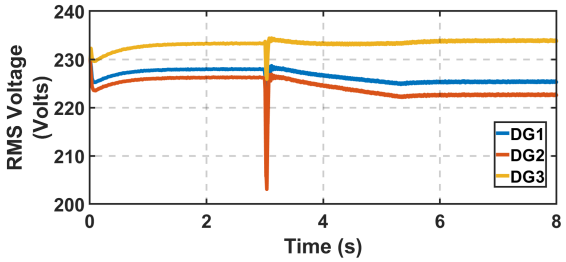

Figure 4.82: RMS voltage of DGs with virtual impedance and with a motor load using opposite droop control

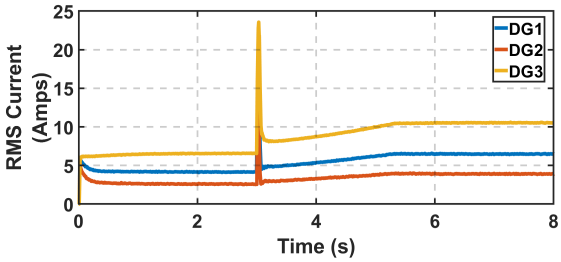

Figure 4.83: RMS current of DGs with virtual impedance and with a motor load using opposite droop control

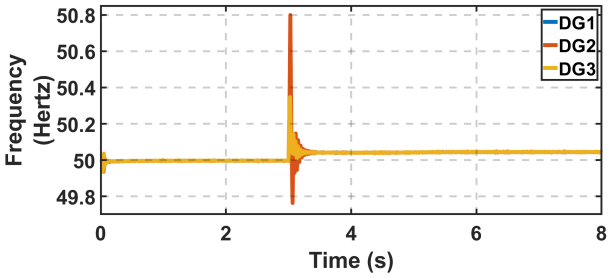

Figure 4.84: Frequency of DGs with virtual impedance and with a motor load using opposite droop control

4.6 Droop controls comparison

Throughout section 4.4 and 4.5 the traditional droop control and the opposite droop control have been tested. When comparing both sections it is possible to draw out the following conclusions. The virtual impedance allows to improve the power sharing in both control schemes at the cost of degrading the voltage to a certain extent. In a low voltage grid with mainly resistive lines and with the virtual impedance both controls have shown to be able to operate correctly. Both controls were able to respond to the changes in the grid that occurred during the tests. However, there is one main differences in the behaviour of these two types of controls that makes one preferable over the other one. This difference is the control of the reactive power. The traditional droop control has a reactive power control that responds to the changes, but not as accurately as desired. The coupling that occurs in the traditional droop control causes the reactive power to have an undesired transient behaviour that often leads to a reactive power sharing that does not correspond to the capacity of each DG. The opposite droop control does not suffer from this coupling. This allows it to respond to the changes in reactive power demand with smoother transients, and keeping the correct power sharing ratio among the DGs. Thus, it is shown that the opposite P.V/Q.F droop control is more suitable for low voltage micro-grids with mainly resistive lines.

Chapter 5

Unbalanced loads

In this chapter the effects of unbalanced loads on the micro-grid are studied. Along with non linear loads, unbalanced loads are one of the two main sources of power quality problems in micro-grids [37]. An unbalanced load is one that causes a difference between the phases of the voltage or differences in the line voltages. One of the most common sources of unbalance is the connection of single phase loads [38]. These single phase loads can be connected between phases or between a phase and ground. Load imbalance between phases tend to occur with more frequency in low voltage networks [39]. Because of the lack of support from the grid, unbalanced loads degrade the power quality of micro-grids. This type of unbalance can lead to abnormal operation by causing vibrations, over-heating, and over-voltage of equipment [40]

In order to analyze the effect of unbalanced loads the sequence components are used. The symmetrical components theory claims that unbalanced three phase quantities can be studied if divided into the positive sequence (PS), negative sequence (NS), and zero sequence components [38]. Unbalance is measured only in terms of the PS and NS quantities. According to [41], the true definition of unbalance is the ratio of the NS voltage over the PS voltage as shown in equation 5.1. This ratio is called the voltage unbalance factor (VUF). According to the International Electrotechnical Commission (IEC) the VUF should be limited to 2 %.

$$\%VUF = \frac{Negative\ sequence\ voltage}{Positive\ sequence\ voltage} * 100 \tag{5.1}$$

One way to compensate for this unbalance is the use of active power filters which compensate by injecting a NS voltage. Yet, for a micro-grid this is not a desirable solution as installing such filters is not an economic solution [40]. Different methods have been proposed to counter unbalance such as using separate DGs as compensators as suggested in [42]. However, the interest in this study is to evaluate the possibility of changing the local control of the DG so that it can reduce the unbalance by compensating the NS.

5.1 Effects on micro-grid control

As introduced before, an unbalanced load brings several negative effects to a micro-grid. This can be further emphasized when the effects on the control of a micro-grid are analyzed. When the grid is in an unbalanced condition the dq components will not be steady and oscillate. Thus, the performance of the droop control will be degraded [43]. Particularly, this can affect the generation of the reference voltage and frequency. This is due to the fact that the voltage and current dq components are used to calculate the active and reactive power fed into the droop control. Even if the power is calculated without using the $dq0$ transformation, there will be problems at the innerloop control level. In section 4.1.2 it was shown that the dq components of the voltage and current are compared to the generated signals and then fed into their respective PI controller. The constant oscillation of the dq components will be reflected in the PI controllers output.

5.2 Sequence decomposition

In order to asses the percentage of voltage unbalance factor it is essential to obtain the positive and negative sequence. It is important to obtain them in a method that does not require being at the fundamental frequency as the system can deviate from it and thus provide inaccurate results. Therefore, in order to avoid this the Notch filtering method is used for symmetrical component decomposition.

This method is done in the $dq0$ frame. It is based on the fact that in such a frame the positive sequence will appear as a DC value. However, the negative sequence will appear as an AC signal. This is because the negative sequence is rotating in the opposite direction to the reference frame [44]. Taking this into consideration, a second order low pass filter can be used to keep only the DC component of the signal which would be the positive sequence. The low-pass filter has the following transfer function

$$LPF = \frac{\omega_c^2}{s^2 + 2\varepsilon\omega_c s + \omega_c^2} \tag{5.2}$$

Where ω_c is the cut-off frequency and ε is the damping ratio. In order to obtain the negative sequence the same procedure can be applied. The main difference being that the $dq0$ transformation the is done using the rotating frame of the negative sequence which is the negative of the positive sequence rotating frame wt. From the obtained signal, the negative sequence will be in the DC component, and the positive component will appear as an AC signal. The same filter as above can be applied in order to obtain the negative sequence.

After the components are extracted, the dq values are used to calculate the voltage unbalance factor. The main positive and negative sequence can be calculated as shown in equations 5.3 and 5.4. These values can then be used to calculate the VUF as shown previously in equation 5.1. The whole process is depicted in figure 5.1

$$V_{dq}^{+} = \sqrt{(v_d^{+})^2 + (v_q^{+})^2} \tag{5.3}$$

$$V_{dq}^{-} = \sqrt{(v_d^{-})^2 + (v_q^{-})^2} \tag{5.4}$$

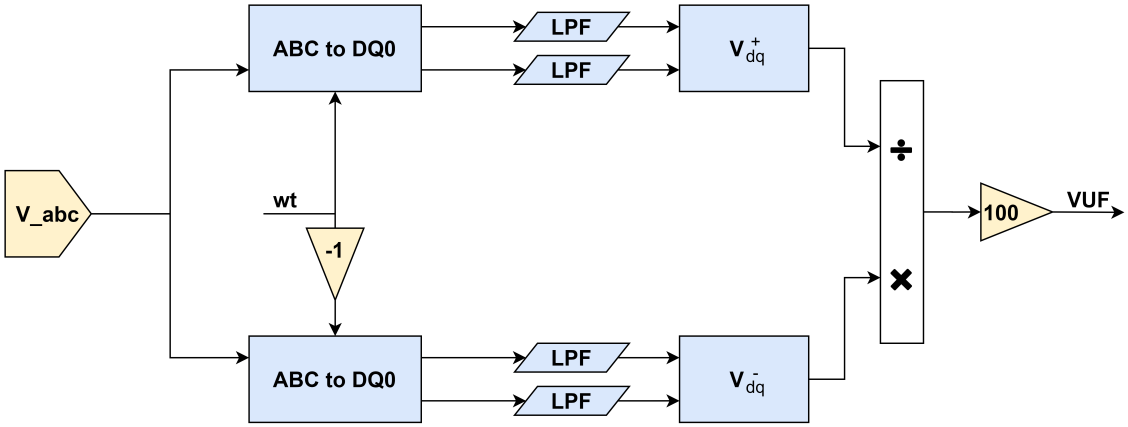

Figure 5.1: Sequence extraction and VUF calculation

5.3 Voltage unbalance compensation

In order to reduce the percentage of VUF a negative sequence compensation system is implemented as shown in [35]. The compensating negative sequence is added to the reference voltage in the voltage control section of the innerloop. The compensation is added at this point as if it is added after to the output of the voltage controller it can be seen as a disturbance by the system [45]. It is important to notice that this method reduces specifically the negative sequence. There can be unbalance situations where the loads cause zero sequence to appear. In order to deal with these situations a different approach is need such as the one shown in [37].

The negative sequence compensating signal is called the Unbalance Compensation reference (UCR), and it is produced in the dq frame. The calculated VUF is compared against a reference level VUF^{*}. This difference is then fed into a PI controller whose output is then multiplied by the dq components of the negative sequence. As shown in figure 5.2 this results in the signal UCR_{dq}.

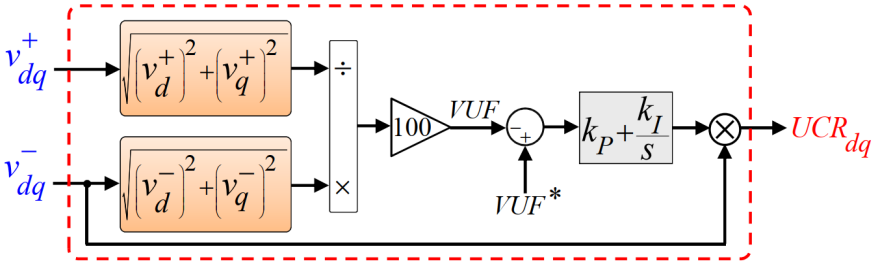

Figure 5.2: Unbalance compensation reference generation [35]

When VUF is bigger than VUF^* the output of the PI controller will be negative. This output is then multiplied with the negative sequence dq components. This results in an inversion of the signals which when added to the reference voltage will result in a compensation. As the compensation is injected into the system, the negative sequence will start decreasing. Therefore, the compensation signal will decrease as well.

Although the innerloop control is done in the $dq0$ frame, the compensation signal UCR_{dq} is not directly used. As mentioned before, the negative sequence appears as an AC signal in the positive sequence. However, UCR_{dq} has been obtained in the rotation frame $-wt$ and thus is a DC signal. In order inject this signal into the innerloop control, it has to be transformed from DC into its equivalent AC signal in the positive sequence. To do this the signal UCR_{dq} is first transformed into the $\alpha\beta$ stationary reference frame. The signal $UCR_{\alpha\beta}$ is calculated using the negative reference $-wt$. Afterwards, this signal is converted back into the dq frame using the positive reference wt. The newly obtained signal is then added to the innerloop control as shown in Figure 5.3.

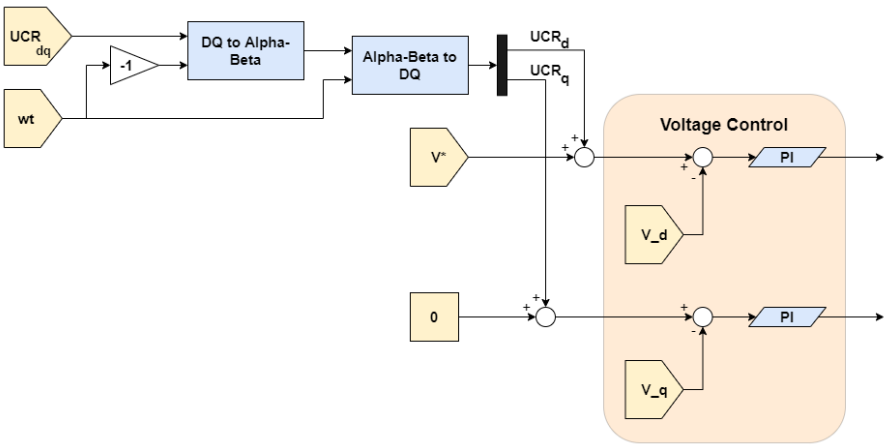

Figure 5.3: Unbalance compensation reference Adaptation

5.4 Area of compensation

As discussed in [35], compensation methods such as the one developed in [45] focus on reducing the VUF measured at the distributed generator. While this is helpful, it is also possible to aim to reduce the VUF at the point of common coupling (PCC). This would be desirable as the loads will tend to actually be connected there. Therefore, it is worthwhile to provide a lower VUF to the loads even if the VUF may increase at the generators. In order to do this the compensation signal UCR_{dq} calculated at the point of common coupling should be sent to the other DGs so that they can inject it into their innerloop control. Because the signal is in the dq frame, sending UCR_{dq} should not require a high bandwidth communication [35]. This approach will be referred to as the low bandwidth communication compensation.

It is important to consider that while the communication requirements are not high, some micro-grids may not have this capability. In order to use this unbalance compensation method without communications a small modification can be made. Instead of using the global signal of the PCC, each DG can calculate its own UCR_{dq} based on its own output voltage and own wt. This approach will be referred to as communication-less compensation. The effectiveness of this communication-less approach will be compared to the low bandwidth communication one in the following sections.

5.5 Simulation results

Using the model described in the previous chapter, the effect of connecting unbalanced loads to the micro-grid is studied. The efficiency of the unbalance compensation method is also tested under different circumstances. The simulations carried out in this section are done using the P.F/Q.V droop control scheme.

5.5.1 Connection of an unbalanced load

First the effect that an unbalanced load causes on the grid is studied. In order to see this the grid shown in figure 4.9 is used. Only load A will be connected which is a load of $8kW$ and $5k$VAR. To showcase the consequences an unbalanced load is connected at $t = 2s$. This unbalanced load is connected as well at the same position of load A which is the PCC. The load consists of a resistive component in parallel with an inductive one. These elements represent a load of $8kW$ and $5k$VAR. This is a single phase load that is connected between phase A and phase B.

First, in figure 5.4 during the stabilization of the system the unbalance starts high, but then decreases until its close to zero. The unbalance during this first part of this stabilization is not shown in order to keep readability. That is why the very first moments the unbalance is set to zero. Afterwards, at $t = 2s$ the single phase load is connected. It can be seen that connecting this load causes the VUF to rise above the recommended 2% threshold. The VUF only goes above the recommended threshold at the PCC. The other DGs are less affected by the unbalanced load.

Figure 5.5 shows the effect the load has on the voltage of DG1. Before its connection, the RMS values of the three phases were aligned. The introduction of the load causes them to have different values.

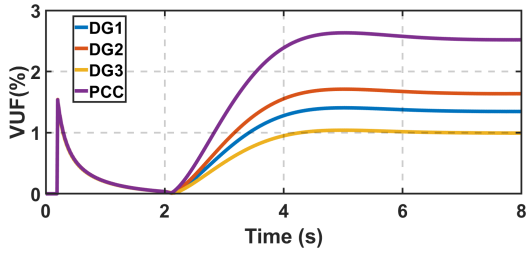

Figure 5.4: Voltage unbalance factor at DGs and PCC with unbalanced load connected at t=2s

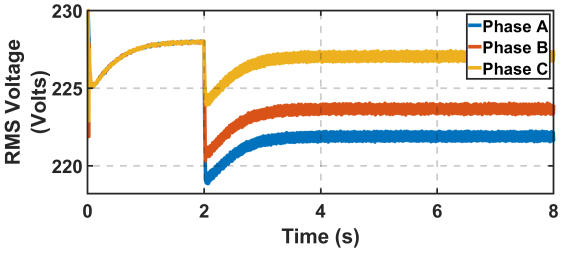

Figure 5.5: RMS Voltage of DG1 with unbalanced load with unbalanced load connected at t=2s

In figures 5.6 and 5.7 the effect the load has on the currents is seen. Before the unbalanced load the three phases of the current have the same amplitude and have an equally spaced phase. The connection of the single phase load causes the amplitude of the phases feeding the load to increase. Additionally, the phases feeding the single phase load are affected by a phase shift. This two effects are linked to the elements that compose the load being connected between the two phases. The unbalanced load has a resistive part that will affect the amplitude of the phases where it is connected. The other part of the unbalanced load is an inductor that due to its nature will induce a phase shift onto the phases its connected to.

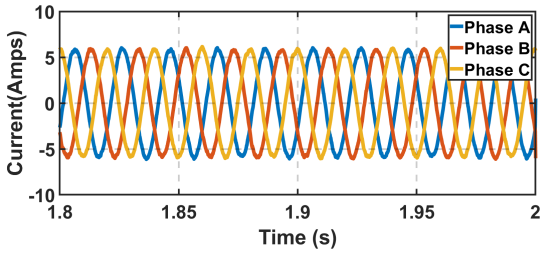

Figure 5.6: Current of DG1 before connection of the unbalanced load

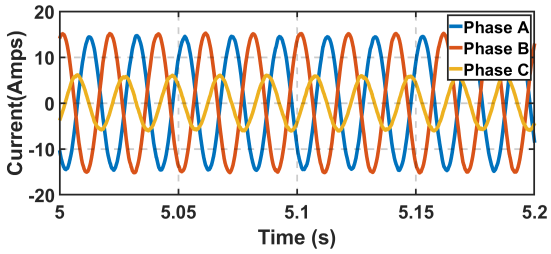

Figure 5.7: Current of DG1 after connection of the unbalanced load

The previously shown non-symmetry in the current and voltage have an effect on the generated active and reactive power. This effect is mainly introducing oscillations into the generated active and reactive power. The quantities shown in figure 5.8 and 5.9 already reflect this oscillation, but it is worth remembering that the shown signals have already been filtered. Furthermore, the low pass filter of the droop control plays an important role under this circumstance. If the power signals are not filtered properly, the big oscillations are subtracted or added to the reference voltage and frequency values. This can make the system oscillate and become more unstable. Therefore the filtering stage of the droop control is important under unbalanced loads. The filter must have a low enough cut-off frequency to prevent the unbalance from deteriorating the control performance. It is important to keep in mind that the innerloop control performance is affected by the unbalanced loads as well. Due to the unbalance the dq0 frame values will not be steady and oscillate. This unsteadiness will cause fluctuations that will affect the PI controller and introduce fluctuations into the reference voltage used for PWM control.

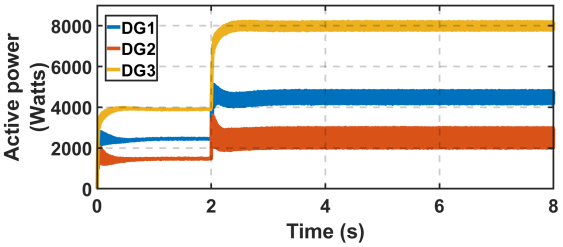

Figure 5.8: Active power generated by DGs with unbalanced load connected at t=2s using traditional droop control

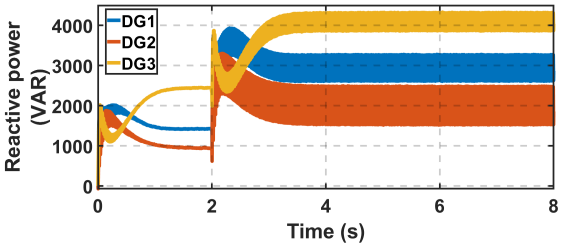

Figure 5.9: Reactive power generated by DGs with unbalanced load connected at t=2s using traditional droop control

5.5.2 Communication-less compensation

In order to test the compensation, the load will be connected at $t = 2s$ as in the previous example. Then the unbalance compensation mechanism will be activated at $t = 5s$ when the VUF is reaching its maximum value. This time of activation is chosen in order to showcase its compensation capabilities. The compensation could be activate before this time and limit the rise of the VUF if desired.

Figure 5.10 shows that the communication-less system is indeed able to reduce the VUF. By having each DG compensate the measured unbalance at their own output, the unbalance at the PCC can be reduced as well. Figure 5.11 demonstrates the effect that the compensation mechanism is having on the voltage DG1. The phases that were separated due to the unbalanced load converge to a same point due to the compensation. Thus returning to a state similar to before the connection of the single phase load.

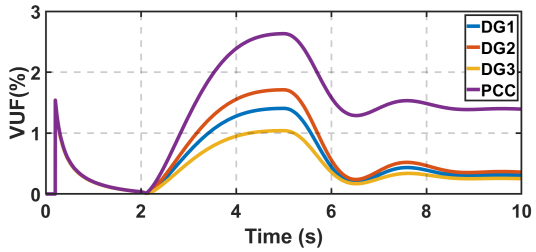

Figure 5.10: VUF with communication-less compensation mechanism activated at t=5s using traditional droop control

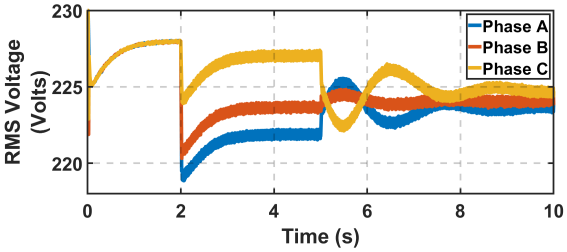

Figure 5.11: RMS Voltage of DG1 with communication-less compensation mechanism activated at t=5s using traditional droop control

As mentioned before, the compensation mechanism can be activated at any time. In figure 5.12 the result obtained when activating the compensation mechanism immediately at $t = 2s$ when the unbalanced load is connected is shown. The simultaneous activation prevents the VUF from reaching the recommended limit of 2% while achieving the same final values of VUF %.

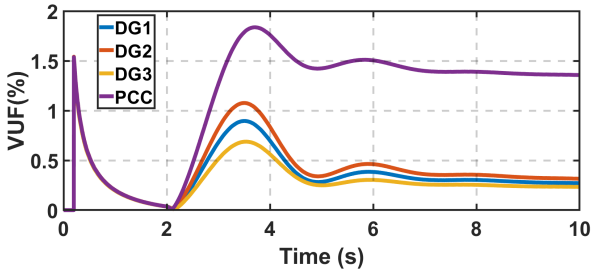

Figure 5.12: VUF with communication-less compensation mechanism activated at t=2s using traditional droop control

5.5.3 Low bandwidth communication compensation

By introducing communication between the PCC and the DGs the UCR_{dq} compensation calculated at the PCC can be send to the DGs. Thus the compensation signals introduced to each DG are intended to reduce the VUF at the PCC rather than the DG. Figure 5.13 shows the response to activating the compensation after the VUF has reached its peak. Meanwhile, figure 5.14 shows the response to activating the compensation at the time when the load is connected. In these figures two main differences can be seen compared to the communication-less compensation. The first one is that the VUF at the PCC can be reduced more by using the low bandwidth communication method. In the communication-less compensation the final value for VUF at the PCC is close to 1.2%. On the other hand, the low bandwidth communication compensation drives the VUF to about 0.5%. This result is closely linked with the second difference. When using the low bandwidth communication compensation, the VUF of the DGs becomes higher rather than decreasing like in the communication-less mode. This occurs because the compensation signals introduced into the innerloop are aiming to reduce the VUF at the PCC and not

the DG itself. Therefore, in order to reduce the VUF at the PCC the DGs increase their own VUF. This can be considered the trade-off of using the low bandwidth communication to further reduce the VUF.

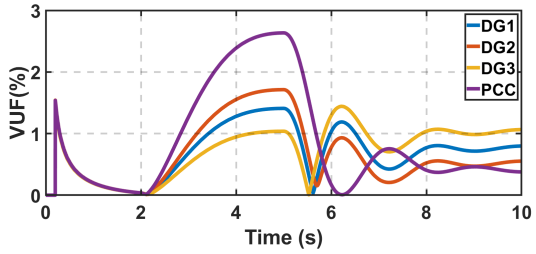

Figure 5.13: VUF with low bandwidth communication compensation mechanism activated at t=5s using traditional droop control

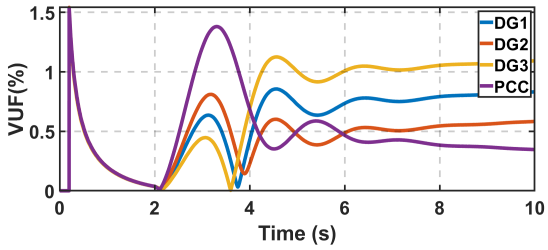

Figure 5.14: VUF with low bandwidth communication compensation mechanism activated at t=2s using traditional droop control

Figure 5.15 shows the evolution of the RMS voltage of DG1. The compensation in this case is introduced at $t = 5s$. As shown in the result of figure 5.13, the VUF of DG1 first increases with the unbalance compensation, but is finally taken to a lower percentage which is shown by the phases becoming closer to each other. On the other hand, figure 5.16 shows the evolution of the RMS voltage of DG3 under the same conditions. DG3 first increases its VUF in order to compensate. However, its final VUF is almost the same as it was before the compensation. Thus, the phases return to their previous positions.

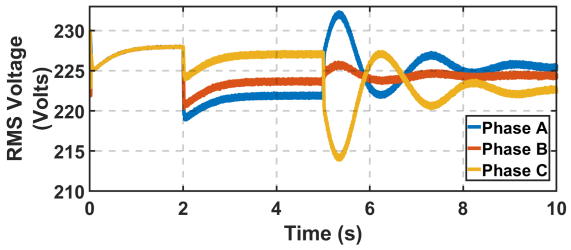

Figure 5.15: RMS Voltage of DG1 with low bandwidth communication compensation mechanism activated at t=5s using traditional droop control

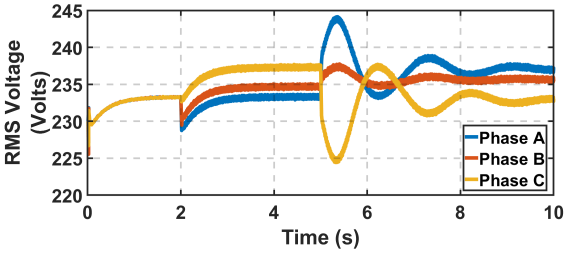

Figure 5.16: RMS Voltage of DG3 with low bandwidth communication compensation mechanism activated at t=5s using traditional droop control

One important detail to remember is that the virtual impedance is also affected by the unbalance. If the current I_g used in the virtual impedance contains both the negative and the positive sequence, the results shown in figures 5.17 and 5.18 are obtained. As mentioned in section 4.3, including the negative sequence will cause the VUF to reach higher levels. This is seen in figure 5.17 where the VUF at the PCC is above 4%. Additionally, compensation will be unevenly shared by the DGs as it is shown in 5.17 and 5.18.

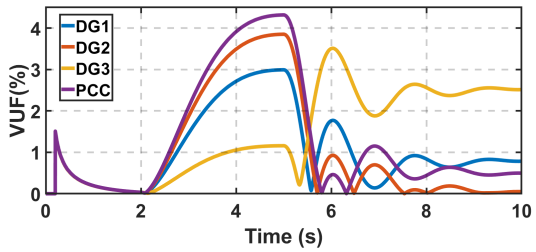

Figure 5.17: VUF with negative sequence in virtual impedance and low bandwidth communication compensation mechanism activated at t=5s using traditional droop control

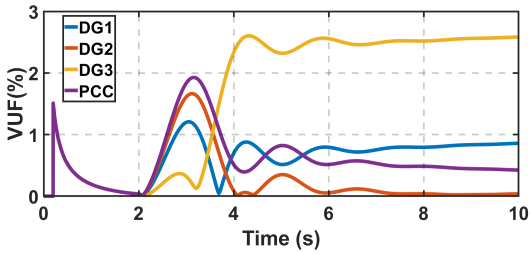

Figure 5.18: VUF with negative sequence in virtual impedance and low bandwidth communication compensation mechanism activated at t=2s using traditional droop control

5.5.4 Unbalance at non-PCC point

In this subsection the effectiveness of both the communication-less and low bandwidth communication mode is evaluated when an unbalanced load is connected at a point different from the PCC. To test this the same unbalanced load is connected next to DG1 at the position of load C as it was shown in figure 4.9. First, figure 5.19 shows that if the unbalanced load is closer to a DG it will affect this DG more than others.

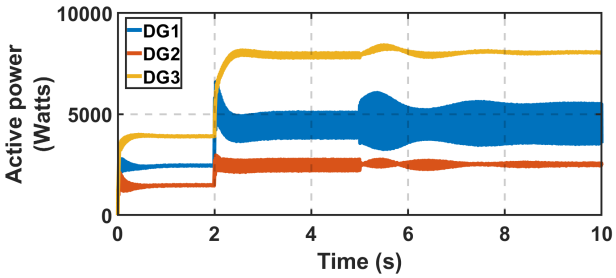

Figure 5.19: Active power generated by DGs with the unbalanced load connected at the position load C at t=2s

The efficiency of the communication-less and the low bandwidth communication compensation are presented in figure 5.20 and figure 5.21 respectively. It can be seen that the obtained final VUF for the unbalanced area (DG1) is similar for both compensation aproaches. The low bandwidth communication compensation is able to reduce it sightly more, but at the cost of increasing the VUF at the other points including the PCC.

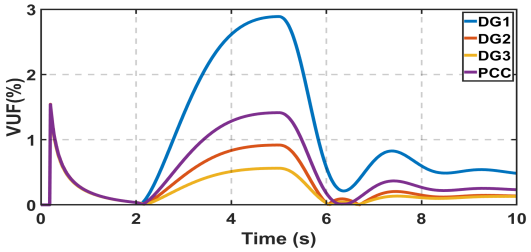

Figure 5.20: VUF with unbalanced load in position B and communication-less compensation mechanism activated at t=5s using traditional droop control

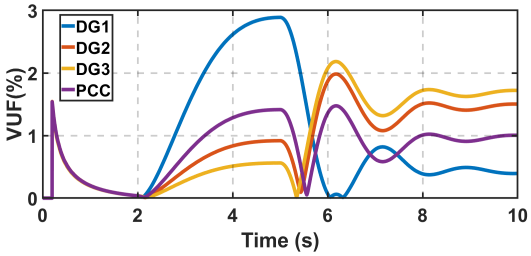

Figure 5.21: VUF with unbalanced load in position B and low bandwidth communication compensation mechanism activated at t=5s using traditional droop control

Figure 5.22 studies the scenario where only the DG of the area affected compensates for the unbalance. Thus, only DG1 is feed an unbalance compensation signal. It is shown that the obtained result is highly similar to the one shown in figure 5.20. This means the same result can be obtained without modifying the other DGs. Thus this could be a viable option under similar situations.

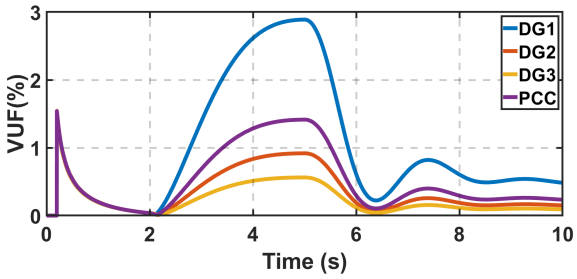

Figure 5.22: VUF compensation with unbalanced load in position B and communication-less compensation mechanism activated only on DG1 at t=5s using traditional droop control

5.6 Simulation results with P.V/Q.F droop control

The simulations done in section 4.5 show that the P.V/Q.F droop control has certain advantages over the P.F/Q.V droop control in a LV grid. This section analyses the compatibility of the P.V/Q.F control method with the unbalance compensation mechanism described in this chapter.

5.6.1 Connection of an unbalanced load

As in the previous test, only load A will be connected which is a load of 8kW and 5kVAR. At $t = 2s$ a single phase load will be connected between phases A and B. This load has an active and reactive power of 8kW and 5kVAR respectively.

As expected, an unbalanced is introduced onto the system which causes oscillations in the generated power. Once again the increased fluctuations can be attributed to the unsteady dq0 values in the innerloop control and to the bigger oscillations introduced by the power into the droop control. The main difference with the P.F/Q.V control scheme is that the reactive power has a smoother transient and is better distributed as seen in figure 5.24. Figure 5.25 shows the measured VUF at the PCC and DGs. The obtained VUF for each location is the same as in the previous scenario.

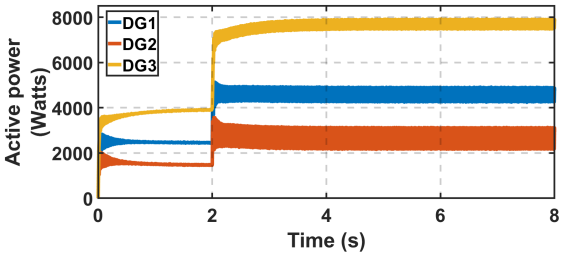

Figure 5.23: Active power generated by DGs with unbalanced load connected at t=2s using opposite droop control

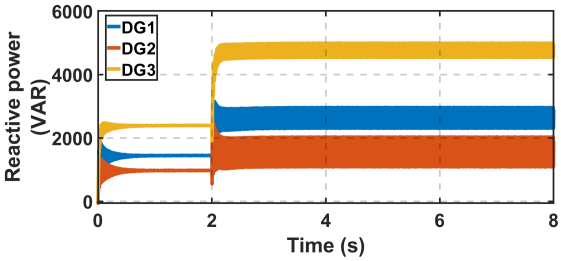

Figure 5.24: Reactive power generated by DGs with unbalanced load connected at t=2s using opposite droop control

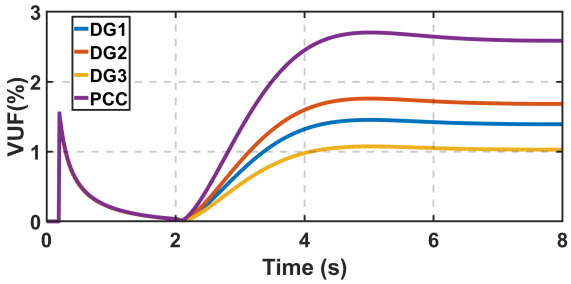

Figure 5.25: Voltage unbalance factor at DGs and PCC with unbalanced load connected at t=2s using opposite droop control

5.6.2 Communication-less compensation

In the first two figures the compensation mechanism is activated at $t = 5s$. The compensation is done with the communication-less approach meaning that every DG is measuring the VUF at their output and is trying to compensate their own measured voltage unbalance.

Figure 5.27 shows the obtained result. The VUF is successfully reduced at each DG and at the PCC as well. Figure 5.27 showcases how the voltage of DG1 improves with the reduction of the voltage unbalance. Figure 5.28 shows the result obtained if the unbalance compensation is activated when the load is connected. The end result is the same, but the initial unbalance caused is mitigated. While these results are good, they do not show any improvement over the compensation done with the P.F/Q.V droop control.

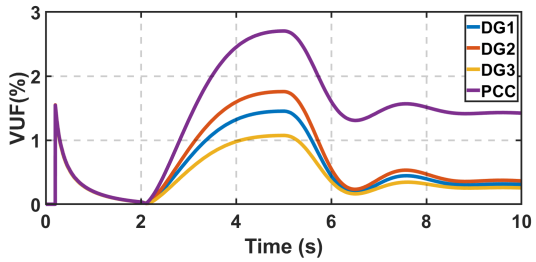

Figure 5.26: VUF with communication-less compensation mechanism activated at t=5s using opposite droop control

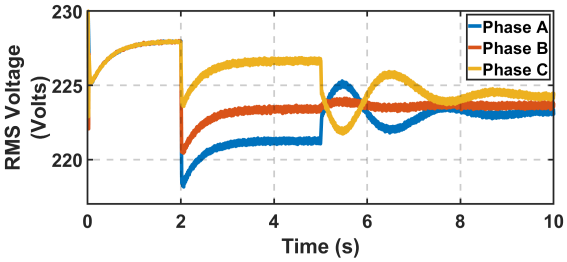

Figure 5.27: RMS Voltage of DG1 with communication-less compensation mechanism activated at t=5s using opposite droop control

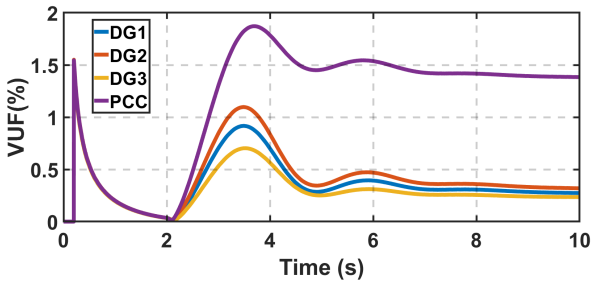

Figure 5.28: VUF with communication-less compensation mechanism activated at t=2s using opposite droop control

5.6.3 Low bandwidth communication compensation

The same scenario is now repeated with the unbalanced load being connected at t=2s, but instead the low bandwidth communication compensation method is used. As explained before, this means that the UCR_{dq} compensation signal calculated at the PCC is sent to each DG. The DGs introduce this signal UCR_{dq} into their innerloop control so that the unbalance at the PCC is reduced. The main results of using this compensation at $t = 5s$ and $t = 2s$ are shown in figure 5.29 and 5.14. The VUF at the PCC is indeed reduced, but in exchange the VUF at the DGs is increased. As it is shown the compensation is done with the same level of accuracy as with the P.F/Q.V droop control.

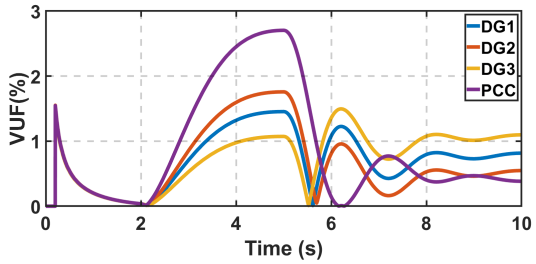

Figure 5.29: VUF with low bandwidth communication compensation mechanism activated at t=5s using opposite droop control

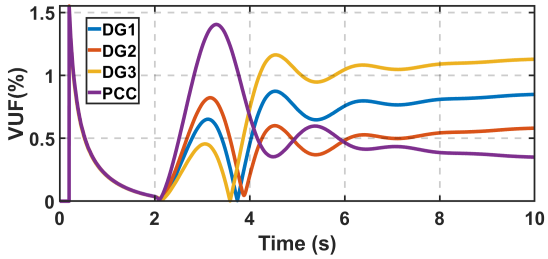

Figure 5.30: VUF with low bandwidth communication compensation mechanism activated at t=2s using opposite droop control

5.6.4 Unbalance at non-PCC point

The compensation at non-PCC points has already been discussed in the subsection 5.5.4. The goal in this subsection is to verify if the performance is affected in any way by the usage of the P.V/Q.F droop control. As it was found in subsection 5.5.4, it is more effective to make only the DG closest to the unbalanced load compensate the VUF. This way the VUF at the other DGs is not unnecessarily increased. Thus, if the unbalanced load is connected next to DG1 only DG1 will participate in the unbalance compensation. The situation previously described is the one tested here. The obtained result is shown in figure 5.31. The system is able to satisfactorily reduce the unbalance at DG1 and at all the other points. The obtained result is the same as the one obtained in subsection 5.5.4. Throughout this section, the results obtained have mimicked the ones obtained in the previous section. These results show that using the P.V/Q.F droop control does not improve the performance of the unbalance compensation. However, it also shows that it does not deteriorate its performance, and thus is compatible with it.

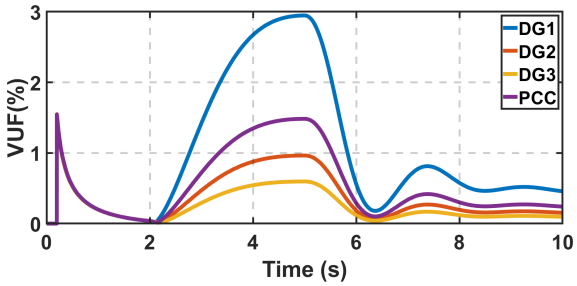

Figure 5.31: VUF compensation with unbalanced load in position B and communication-less compensation mechanism activated only on DG1 at t=5s using opposite droop control

5.7 Unbalance compensation methods comparison

In the last two section the low bandwidth communication and the communication-less compensation mechanisms were tested. From the obtained results their performance can assessed and compared. When the unbalanced load is located at the PCC both methods are able to reduce the VUF. However, the low bandwidth communication mechanism is able to reduce it more than the communication-less at the cost of increasing the VUF at the DGs. If the unbalanced load is not located at the PCC the communication-less mechanism shows a better performance. Although the low bandwidth mechanism can reduce the VUF at a non-PCC location to the same degree as the communication-less, the communication-less mechanism does not increase the VUF at the other DGs. The final result obtained showed that for points different from the PCC it is enough to have only the DG close to the unbalanced load compensate for the negative sequence with the communication-less approach. This allows to have less DGs compensating while retaining the same performance. The final result that was obtained from the tests is that both the traditional and opposite droop controls are compatible with the unbalance compensation mechanism. Furthermore, the performance of the compensation is independent from the type of droop control used.

Chapter 6

Conclusion and future work

Conclusion

Several efforts are being made in order to provide electricity to rural areas that are in the process of developing. Due to the decentralized population and geographical context of theses rural areas expanding the grid can be a very expensive or a non-viable option. In this context, micro-grids provide a way to bring electricity to such areas. Micro-grids provide more capabilities than smaller off-grid sources and can even merge with the grid eventually. One key component of these micro-grids is the usage of distributed generators (DG). The DGs used in many cases are renewable energies. The continuous drop in prices of renewable energies such as wind and solar is making them a more accessible and clean source of energy suitable for remote locations. Thus, the inclusion of renewable energies into the micro-grid is more common and desired. Unfortunately, this inclusion introduces more challenges and questions into the control and efficiency of the micro-grid.

The main challenges of micro-grids is managing the voltage and frequency of the grid. The lack of inertia and low amount of generators make it difficult to set this values. These challenges are managed through the control algorithm of the DGs. The DGs can act as grid-forming (setting the voltage and frequency), grid-supporting (feeding power), or grid-supporting (regulate voltage and current while feeding power). In order to coordinate the different types of DGs communication between them can be needed. However, in this study control algorithms without communications were favored for their simplicity and reliability. Thus, a grid with only grid-supporting units was established.

In this context two control schemes were compared the "traditional" P.F/Q.V droop control and the "opposite" P.V/Q.F droop control. Due to their reduced size, micro-grids have mainly resistive lines. It was shown that this mainly resistive impedance has an impact on the accuracy of the traditional droop control scheme. While the usage of a virtual impedance is able to improve the performance, the coupling formed between the P.F and the Q.V droop controls causes undesired results. Meanwhile, the opposite droop control scheme showed a better handling of the active and reactive power responses. The

usage of a virtual impedance further improved the performance of the P.V/Q.F droop control, and helped avoid inaccuracies in the load sharing among DGs. It was shown that both control schemes and the proposed micro-grid were able to handle different scenarios such as disconnections, and the starting of an induction motor. When comparing the traditional control versus the opposite control, it is apparent that in mainly resistive lines the opposite droop control performs better. The opposite droop control presents smoother transients, and it reaches the final value after each transient faster. Since its active power droop is not coupled with its reactive power droop control, it does not show undesired changes when increasing one quantity, which is the case of the traditional droop control.

The final chapter of the thesis discussed how to mitigate the impact of unbalanced loads. The unbalanced studied was caused by a single phase load connected between phases A and B. This type of connection causes an increase in the voltage negative sequence. It deteriorates the power quality of the micro-grid and leads to abnormal operation of the micro-grid. The compensation method studied focuses on having the DGs themselves compensate this unbalance by adding a compensation negative sequence signal. This is done with the objective to reduce the voltage unbalance factor (VUF). While the proposed method requires a level of communication, it was studied as well if it could operate in a communication-less approach. The first scenario studied was a single phase load connected at the PCC. It was possible to reduce the unbalance with the communication-less compensation. However, the low bandwidth communication compensation was able to further reduce the VUF at the PCC at the cost of increasing the VUF at each DG. The second scenario discussed was the connection of an unbalanced load to a non-PCC area. In other words, connecting the single phase load at the output of a DG. It was shown that the communication-less and low bandwidth communication schemes reduced the VUF to the same degree at the point where the unbalanced load was connected. However, the low bandwidth communication compensation causes the VUF to rise at the other DGs and PCC. Furthermore, it was found that the same level of VUF reduction can be achieved while having only the affected DG compensate the negative sequence with the communication-less aproach. The unbalance compensation tests were repeated with the P.V/Q.F droop control to see if the performance was affected in any way. The obtained results where the same. Therefore, it was proved that the P.V/Q.F droop control is compatible with this negative sequence compensation scheme.

Future work

In this study the power coming from photo-voltaic panels was assumed to be constant. One next step could be to explore how would the system act if the max power from the source is changing with time. This could lead to the usage of an adaptive droop coefficient. Additionally, energy storage devices where not taken into account. They could be added in order to increase the complexity and realism of the system.

During the simulations, it was also found that it is possible to have some DGs operating under the P.F/Q.V droop while others act on the P.V/Q.F droop scheme. It could be studied if having these two control schemes mixed could lead to operational advantages. This would lead to some DGs that excel at providing active power accurately while others excel at providing reactive power accurately.

In terms of unbalance only the negative sequence was discussed here. However, there are loads that can lead to a zero sequence increase that disrupts the grid. One next step would be to study whether the control of the DGs can be modified to compensate for both negative and zero sequences.

Bibliography

[1] G. Venkataramanan and S. Bala, "Resource Aggregation Using Microgrids", en, in *Power Electronics for Renewable and Distributed Energy Systems: A Sourcebook of Topologies, Control and Integration*, ser. Green Energy and Technology, S. Chakraborty, M. G. Simões, and W. E. Kramer, Eds., London: Springer London, 2013, pp. 469–491, ISBN: 978-1-4471-5104-3. DOI: 10.1007/978-1-4471-5104-3_12.

[2] IEA, IRENA, UNSD, WB, and WHO, "Tracking sdg7: The energy progress report", 2019. [Online]. Available: https://trackingsdg7.esmap.org/data/files/download-documents/2019-Tracking%5C%20SDG7-Full%5C%20Report.pdf.

[3] H. Louie, *Off-grid electrical systems in developing countries*, en. New York, NY: Springer Science+Business Media, 2018, ISBN: 978-3-319-91889-1.

[4] I. E. Agency, *Energy Access Outlook 2017: From Poverty to Prosperity*. IEA, 2017.

[5] I. R. E. Agency, *Renewable Power Generation Costs in 2018*. IRENA, 2018, ISBN: 978-92-9260-126-3.

[6] IEA, "Renewables 2018", 2018. [Online]. Available: https://www.iea.org/reports/renewables-2018.

[7] B. Martin, "Autonomous microgrids for rural electrification : Joint investment planning of power generation and distribution through convex optimization", en, PhD thesis, UCL - Université Catholique de Louvain, 2018.

[8] Energy Sector Management Assistance Program, *Mini Grids for Half a Billion People: Market Outlook and Handbook for Decision Makers*, en. World Bank, Jun. 2019. DOI: 10.1596/31926. [Online]. Available: http://elibrary.worldbank.org/doi/book/10.1596/31926.

[9] Q. Shafiee, J. M. Guerrero, and J. C. Vasquez, "Distributed secondary control for islanded microgrids—A novel approach", *IEEE Transactions on power electronics*, vol. 29, no. 2, pp. 1018–1031, 2013.

[10] F. Katiraei, R. Iravani, N. Hatziargyriou, and A. Dimeas, "Microgrids management", *IEEE power and energy magazine*, vol. 6, no. 3, pp. 54–65, 2008.

[11] H. Lotfi and A. Khodaei, "AC versus DC microgrid planning", *IEEE Transactions on Smart Grid*, vol. 8, no. 1, pp. 296–304, 2015.

[12] J. M. Guerrero, J. C. Vasquez, J. Matas, L. G. De Vicuña, and M. Castilla, "Hierarchical control of droop-controlled AC and DC microgrids—A general approach toward standardization", *IEEE Transactions on industrial electronics*, vol. 58, no. 1, pp. 158–172, 2010.

[13] J. J. Justo, F. Mwasilu, J. Lee, and J.-W. Jung, "AC-microgrids versus DC-microgrids with distributed energy resources: A review", *Renewable and sustainable energy reviews*, vol. 24, pp. 387–405, 2013.

[14] J. Rocabert, A. Luna, F. Blaabjerg, and P. Rodríguez, "Control of Power Converters in AC Microgrids", *IEEE Transactions on Power Electronics*, vol. 27, no. 11, pp. 4734–4749, Nov. 2012, ISSN: 1941-0107. DOI: 10.1109/TPEL.2012.2199334.

[15] T. Vandoorn, J. De Kooning, B. Meersman, and L. Vandevelde, "Review of primary control strategies for islanded microgrids with power-electronic interfaces", en, *Renewable and Sustainable Energy Reviews*, vol. 19, pp. 613–628, Mar. 2013, ISSN: 13640321. DOI: 10.1016/j.rser.2012.11.062. [Online]. Available: https://linkinghub.elsevier.com/retrieve/pii/S1364032112006764.

[16] J. P. Lopes, C. L. Moreira, and A. G. Madureira, "Defining control strategies for microgrids islanded operation", *IEEE Transactions on power systems*, vol. 21, no. 2, pp. 916–924, 2006.

[17] A. Engler, "Control of parallel operating battery inverters", in *Photovoltaic Hybrid Power Systems Conference*, 2000, pp. 1–4.

[18] M. Hedayatpour and A. Mirzaei, "Control Methods in Microgrids", in, Dec. 2018.

[19] A. M. Bollman, "An experimental study of frequency droop control in a low-inertia microgrid", 2010.

[20] X. Hou, Y. Sun, W. Yuan, H. Han, C. Zhong, and J. Guerrero, "Conventional P-w/Q-V Droop Control in Highly Resistive Line of Low-Voltage Converter-Based AC Microgrid", en, *Energies*, vol. 9, no. 11, p. 943, Nov. 2016, ISSN: 1996-1073. DOI: 10.3390/en9110943. [Online]. Available: http://www.mdpi.com/1996-1073/9/11/943.

[21] Y. Zhu, F. Zhuo, B. Liu, and H. Yi, "An enhanced load power sharing strategy for low-voltage microgrids based on inverse-droop control method", in *2014 International Power Electronics Conference (IPEC-Hiroshima 2014 - ECCE ASIA)*, ISSN: 2150-6086, May 2014, pp. 3546–3552. DOI: 10.1109/IPEC.2014.6870006.

[22] M. Salcone and J. Bond, "Selecting film bus link capacitors for high performance inverter applications", en, in *2009 IEEE International Electric Machines and Drives Conference*, Miami, FL, USA: IEEE, May 2009, pp. 1692–1699, ISBN: 978-1-4244-4251-5. DOI: 10.1109/IEMDC.2009.5075431. [Online]. Available: http://ieeexplore.ieee.org/document/5075431/.

[23] R. Albarracín and M. Alonso, "Photovoltaic reactive power limits", in *2013 12th International Conference on Environment and Electrical Engineering*, 2013, pp. 13–18.

[24] M. Dursun and M. K. DÖŞOĞLU, "LCL Filter Design for Grid Connected Three-Phase Inverter", in *2018 2nd International Symposium on Multidisciplinary Studies and Innovative Technologies (ISMSIT)*, IEEE, 2018, pp. 1–4.

[25] A. Kahlane, L. Hassaine, and M. Kherchi, "LCL filter design for photovoltaic grid connected systems", *the Journal of Renewable Energies*, pp. 227–232, 2014.

[26] A. H. Javed, M. A. Amin, T. Iqbal, and N. Ali, "Power Sharing through Droop Control for Parallel Inverters with Line impedance Effect", en, *Environment and Sustainable Development*, p. 11, 2016.

[27] A. El Moubarek Bouzid, P. Sicard, A. Yamane, and J.-N. Paquin, "Simulation of droop control strategy for parallel inverters in autonomous AC microgrids", en, in *2016 8th International Conference on Modelling, Identification and Control (ICMIC)*, Algiers, Algeria: IEEE, Nov. 2016, pp. 701–706, ISBN: 978-0-9567157-7-7. DOI: 10.1109/ICMIC.2016.7804202. [Online]. Available: http://ieeexplore.ieee.org/document/7804202/.

[28] Dan Wu, Fen Tang, J. C. Vasquez, and J. M. Guerrero, "Control and analysis of droop and reverse droop controllers for distributed generations", en, in *2014 IEEE 11th International Multi-Conference on Systems, Signals & Devices (SSD14)*, Castelldefels-Barcelona, Spain: IEEE, Feb. 2014, pp. 1–5, ISBN: 978-1-4799-3866-7. DOI: 10.1109/SSD.2014.6808842. [Online]. Available: http://ieeexplore.ieee.org/document/6808842/.

[29] K. Duwadi, "Simulation for parallel operation of inverters with frequency and voltage droop control", en, 2015. DOI: 10.13140/RG.2.1.1918.3203. [Online]. Available: http://rgdoi.net/10.13140/RG.2.1.1918.3203.

[30] A. Khaledian and M. Aliakbar Golkar, "Analysis of droop control method in an autonomous microgrid", en, *Journal of Applied Research and Technology*, vol. 15, no. 4, pp. 371–377, Aug. 2017, ISSN: 16656423. DOI: 10.1016/j.jart.2017.03.004. [Online]. Available: http://www.jart.icat.unam.mx/index.php/jart/article/view/678.

[31] R. An, J. Liu, T. Wu, S. Wang, and B. Liu, "Analysis and design of cutoff frequency for power calculation low-pass filters in droop control", in *2017 IEEE 3rd International Future Energy Electronics Conference and ECCE Asia (IFEEC 2017 - ECCE Asia)*, ISSN: null, Jun. 2017, pp. 1596–1600. DOI: 10.1109/IFEEC.2017.7992285.

[32] A. Engler and N. Soultanis, "Droop control in LV-grids", in *2005 International Conference on Future Power Systems*, IEEE, 2005, 6–pp.

[33] A. Micallef, M. Apap, C. Spiteri-Staines, and J. M. Guerrero, "Performance comparison for virtual impedance techniques used in droop controlled islanded microgrids", in *2016 International Symposium on Power Electronics, Electrical Drives, Automation and Motion (SPEEDAM)*, Jun. 2016, pp. 695–700. DOI: 10.1109/SPEEDAM.2016.7526013.

[34] P. L. Minh, H. P. T. Xuan, D. H. V. Duc, and H. N. Minh, "Control of power sharing in an island microgrid using virtual impedance", in *2017 International Conference on System Science and Engineering (ICSSE)*, ISSN: 2325-0925, Jul. 2017, pp. 154–159. DOI: 10.1109/ICSSE.2017.8030856.

[35] M. Savaghebi, A. Jalilian, J. C. Vasquez, and J. M. Guerrero, "Secondary control scheme for voltage unbalance compensation in an islanded droop-controlled microgrid", *IEEE Transactions on Smart Grid*, vol. 3, no. 2, pp. 797–807, 2012.

[36] H. Han, Y. Liu, Y. Sun, M. Su, and J. M. Guerrero, "An improved droop control strategy for reactive power sharing in islanded microgrid", *IEEE Transactions on Power Electronics*, vol. 30, no. 6, pp. 3133–3141, 2014.

[37] F. Najafi, M. Hamzeh, and M. Fripp, "Unbalanced Current Sharing Control in Islanded Low Voltage Microgrids", en, *Energies*, vol. 11, no. 10, p. 2776, Oct. 2018, ISSN: 1996-1073. DOI: 10.3390/en11102776. [Online]. Available: http://www.mdpi.com/1996-1073/11/10/2776.

[38] M. Savaghebi, A. Jalilian, J. C. Vasquez, and J. M. Guerrero, "Autonomous voltage unbalance compensation in an islanded droop-controlled microgrid", *IEEE Transactions on Industrial Electronics*, vol. 60, no. 4, pp. 1390–1402, 2012.

[39] G. M. D. S. Azevedo, J. Rocabert, M. C. Cavalcanti, F. D. A. D. S. Neves, and P. Rodríguez, "A negative-sequence current injection method to mitigate voltage imbalances in microgrids", *Eletrônica de Potência*, vol. 16, no. 4, pp. 296–303, Jan. 2011. DOI: 10.18618/rep.20114.296303.

[40] Q. Liu, Y. Tao, X. Liu, Y. Deng, and X. He, "Voltage unbalance and harmonics compensation for islanded microgrid inverters", 2014. DOI: 10.1049/iet-pel.2013.0410.

[41] P. Pillay and M. Manyage, "Definitions of voltage unbalance", *IEEE Power Engineering Review*, vol. 21, no. 5, pp. 50–51, 2001.

[42] F. Shahnia, R. Majumder, A. Ghosh, G. Ledwich, and F. Zare, "Operation and control of a hybrid microgrid containing unbalanced and nonlinear loads", *Electric Power Systems Research*, vol. 80, no. 8, pp. 954–965, 2010.

[43] M. S. Golsorkhi and D. D. C. Lu, "A decentralized negative sequence compensation method for islanded mirogrids", in *2015 IEEE 6th International Symposium on Power Electronics for Distributed Generation Systems (PEDG)*, IEEE, 2015, pp. 1–7.

[44] T. Hao, F. Gao, and T. Xu, "Fast Symmetrical Component Extraction From Unbalanced Three-Phase Signals Using Non-Nominal *dq* -Transformation", en, *IEEE Transactions on Power Electronics*, vol. 33, no. 11, pp. 9134–9141, Nov. 2018, ISSN: 0885-8993, 1941-0107. DOI: 10.1109/TPEL.2018.2822941. [Online]. Available: https://ieeexplore.ieee.org/document/8331121/.

[45] M. Savaghebi, J. M. Guerrero, A. Jalilian, and J. C. Vasquez, "Experimental evaluation of voltage unbalance compensation in an islanded microgrid", en, in *2011 IEEE International Symposium on Industrial Electronics*, Gdansk, Poland: IEEE, Jun. 2011, pp. 1453–1458, ISBN: 978-1-4244-9310-4. DOI: 10.1109/ISIE.2011.5984374. [Online]. Available: http://ieeexplore.ieee.org/document/5984374/.

UNIVERSITÉ CATHOLIQUE DE LOUVAIN
École polytechnique de Louvain
Rue Archimède, 1 bte L6.11.01, 1348 Louvain-la-Neuve, Belgique | **www.uclouvain.be/epl**